

REPORT DOCUMENTATION

AFRL-SR-BL-TR-98-

Approved
10. 0704-0188

Public reporting burden for this collection of information is estimated to average 1 h gathering and maintaining the data needed, and completing and reviewing the collection of information, including suggestions for reducing this burden, to Washington, Davis Highway, Suite 1204, Arlington, VA 22202-4302, and to the Office of Management

archiving existing data sources, site or any other aspect of this and Reports, 1215 Jefferson Station, DC 20503.

1. AGENCY USE ONLY (Leave blank)

2. REPORT DATE

FINAL 01 Sep 97 To 28 Feb 98

4. TITLE AND SUBTITLE

DEVELOPMENT OF HIGHLY ACTIVE ELECTRO-OPTIC POLYMERS FOR IN-LINE FIBER PHOTONIC DEVICES

5. FUNDING NUMBERS

F49620-97-C-0060

STTR/TS

65502F

6. AUTHOR(S)

DR RICHARD A. HILL

7. PERFORMING ORGANIZATION NAME(S) AND ADDRESS(ES)

Optivision, Inc.
3450 Hillview Ave
Palo Alto CA 94304

8. PERFORMING ORGANIZATION REPORT NUMBER

9. SPONSORING / MONITORING AGENCY NAME(S) AND ADDRESS(ES)

AFOSR/NL
110 Duncan Ave Room b115
Bolling AFB DC 20332-8050

10. SPONSORING / MONITORING AGENCY NUMBER

Dr Charles Y-C. Lee

11. SUPPLEMENTARY NOTES

19980602 088

12a. DISTRIBUTION / AVAILABILITY STATEMENT

Approved for public release;
distribution unlimited.

12b. DISTRIBUTION CODE

13. ABSTRACT (Maximum 200 words)

Optivision has completed a Phase I STTR project with the objective of developing highly active, electro-optic (EO) polymers tailored for use in in-line fiber photonic devices. The specific Phase I tasks were: (1) Synthesize or obtain a quantity of "development" polymer. (2) Develop suitable processing and characterization methodologies. (3) Perform device level testing of EO polymers using a polymeric in-line fiber (PILF) structure. (4) Identify suitable nonlinear optical (NLO) chromophores for resonantly enhanced EO polymers. (5) Develop a synthesis strategy for novel highly active EO polymers to be produced during Phase II. (6) Perform a high level design of a device to be built during the Phase II effort. We have successfully completed all of these tasks. We have developed new EO polyquinoline materials specifically tailored for use in PILF structures and demonstrated the use of these polymers in actual PILF devices. The new polyquinolines incorporate chromophores with large UB values and red shifted absorption peaks, resulting in polymers with EO coefficients of approximately 30 pm/V at a wavelength of 1.3 um.

14. SUBJECT TERMS

DTIC QUALITY INSPECTED 4

15. NUMBER OF PAGES

16. PRICE CODE

17. SECURITY CLASSIFICATION OF REPORT

(U)

18. SECURITY CLASSIFICATION OF THIS PAGE

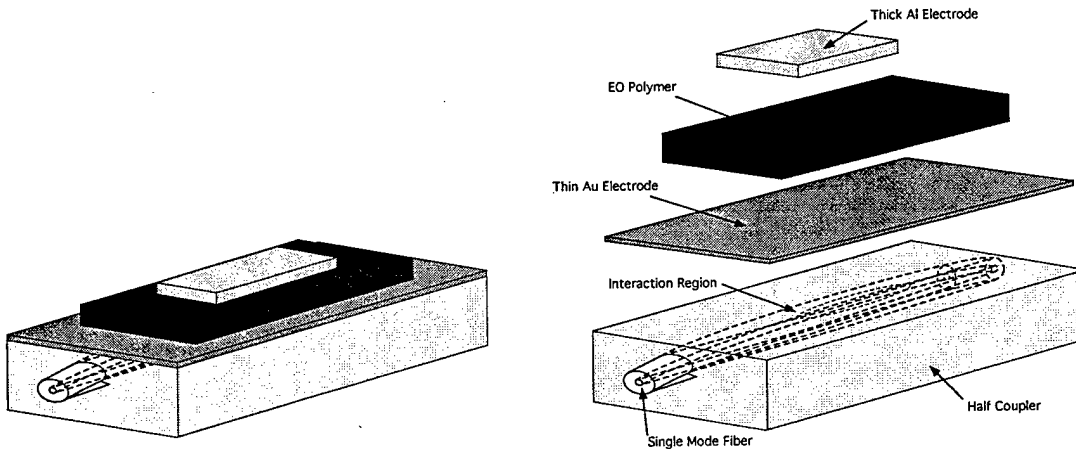
(U)

19. SECURITY CLASSIFICATION OF ABSTRACT

(U)

20. LIMITATION OF ABSTRACT

(UL)



Contract Title: **Development of Highly Active Electro-Optic Polymers for In-Line Fiber Photonic Devices**

Contract No.: F49620-97-C-0060

Report Title: **Final Report**

Reporting Period: 1 September 1997 to 28 February 1998

Due Date: **31 March 1998**

Contract Period: 1 September 1997 to 28 February 1998

Issuing/Monitoring Agency: **AFOSR**

Name of Contractor: **Optivision, Inc.**

Principal Investigator: Dr. Richard A. Hill

Address: 3450 Hillview Ave., Palo Alto, CA 94304

Phone Number: (650) 855-0200

Fax Number: (650) 855-0222

Email: hill@optivision.com

WARNING

This document contains technical data whose export is restricted by the Arms Export Control Act (Title 22, U.S.C., Sec 2751, et seq.) or the Export Administration Act of 1979, as amended, Title 50, U.S.C., App. 2401, et seq. Violations of these export laws are subject to severe criminal penalties. Disseminate in accordance with the provisions of AFR 80-34.

Table of Contents

| | |
|------------------------------------------------------------|----|
| 1. Executive Summary..... | 5 |
| 2. Introduction..... | 7 |
| 2.1 Project Scope..... | 7 |
| 2.2 Technical Objectives..... | 8 |
| 2.3 Report Organization | 9 |
| 3. Overview of Structure Architecture | 10 |
| 4. Electro-Optic Polyquinolines | 14 |
| 5. Processing and Characterization Methodology | 16 |
| 5.1 Guest-Host Polyquinoline..... | 16 |
| 5.2 Processing and Characterization | 17 |
| 5.2.1 Linear Optical Properties | 17 |
| 5.2.2 Nonlinear Optical Properties..... | 18 |
| 5.2.3 Temporal Stability..... | 21 |
| 5.2.4 Thermal Conductivity..... | 22 |
| 6. PILF Structure Fabrication and Evaluation | 24 |
| 6.1 Structure Modeling | 24 |
| 6.2 Liftoff Deposition of EO polymer film..... | 25 |
| 6.3 PILF Structure Fabrication | 27 |
| 6.4 Modified Fabrication Procedure | 30 |
| 6.5 PILF Spurious Free Dynamic Range..... | 32 |
| 7. Synthesis of Highly Active Electro-Optic Polymers | 38 |
| 7.1 Motivation | 38 |
| 7.2 Nonlinear Optical Chromophores..... | 41 |
| 8. Future Work | 45 |
| 8.1 Development of Highly Active EO Polymers | 45 |
| 8.2 Material Characterization..... | 48 |
| 8.2.1 Linear and Nonlinear Optical Properties..... | 48 |
| 8.2.2 Long Term Stability..... | 48 |
| 8.3 PILF Device Development..... | 49 |
| 8.4 Commercialization Plan..... | 50 |
| 8.5 Conclusions | 52 |
| 9. References | 53 |

Table of Figures

| | |
|--------------------------------------------------------------------------------------------------------------------------------------------------------------------------------------------------------------------------------------------------------------------------------------------------------------------------------------------------------------------------------------------------------------------------------------------------------------------------------------------|----|
| Figure 1. Polymeric in-line fiber (PILF) structure. The exploded view on the right clearly shows the curved fiber path and the interaction region where a portion of the fiber cladding is removed to gain access to the evanescent fields..... | 10 |
| Figure 2. Cross section of the PILF structure shown in Figure 1..... | 10 |
| Figure 3. PILF device operation. A top view of the device is shown in (a) and illustrates the diffraction that occurs in the planar waveguide overlay. (b) shows a side view and represents the coupling from the embedded fiber into the waveguide overlay. For the sake of clarity, electrodes are omitted from both figures. | 11 |
| Figure 4. Representation of the transmission spectrum (transmitted power vs. wavelength) of a PILF structure illustrating the dip at the phase matching wavelength. The two curves represent the effect of voltage tuning the phase matched wavelength..... | 12 |
| Figure 5. Chemical synthesis of fluorinated polyquinoline. | 15 |
| Figure 6. Chemical structure of both the (a) polyquinoline host and (b) dibutylaminobezene-thiophene stilbene tricyanovinyl guest of the mixture that was used as a "development" polymer. The chromophore concentration was 25 % by weight..... | 16 |
| Figure 7. Refractive indices of the guest-host polymer as measured by spectroscopic ellipsometry. The upper curve is the extraordinary index while the lower curve is the ordinary index | 17 |
| Figure 8. Absorption spectrum of the polyquinoline guest-host normalized to a 1 μm film thickness. The absorption peak is significantly red-shifted and located at approximately 690 nm. | 18 |
| Figure 9. Experimental configuration for the dispersive measurement of the Pockels coefficient using a Fabry-Perot reflection modulator. The photodetector signal is sent to two separate lock-in amplifiers. The sync signal from the chopper is sent to one lock-in to detect the intensity of the light reflected from the Fabry-Perot structure. The sync signal of the signal generator is sent to the other lock-in to detect the light modulated by the Fabry-Perot structure | 19 |
| Figure 10. Reflected and modulated intensities measured with the Fabry-Perot structure at 1.064 μm (TM polarization shown, TE is similar)..... | 20 |
| Figure 11. Temporal stability of the guest-host mixture at a temperature of 80 $^{\circ}\text{C}$. After an initial decay, the measure EO coefficient was stable for more than 1000 hours. | 21 |
| Figure 12. Resistivity and Conductivity of the polyquinoline guest-host polymer..... | 22 |
| Figure 13. Measured second harmonic signal vs. temperature during both poling (field applied) and depoling (no field applied). Also shown is the poling current as a function of temperature. | 23 |

| | |
|------------------------------------------------------------------------------------------------------------------------------------------------------------------------------------------------------------------------------------------------------------------------------------------------------------------------------------------------------------------------------------------------------|----|
| Figure 14. Simulation of the transmission through a PILF structure fabricated with standard half-coupler, a 10 nm gold lower electrode, a 2.03 μm thick polyquinoline layer, and a 200 nm thick aluminum upper electrode. These design parameters result in phase matching at a wavelength of 1.3 μm | 24 |
| Figure 15. Liftoff deposition technique for the preparation of PILF structures. The EO polymer film is completely prepared, including poling and deposition of metal electrodes, on a temporary substrate and then transferred to the half-coupler block. . | 26 |
| Figure 16. Experimental configuration used for preliminary evaluation of PILF modulator structures. | 27 |
| Figure 17. Transmission spectrum of the polyquinoline PILF structure. The solid line is the measured data while the dashed line is a theoretical fit. The discrepancy at low levels is due to the noise floor of the optical spectrum analyzer. The star represents the wavelength of a common communications laser, 1.319 μm | 28 |
| Figure 18. Theoretical modulation spectrum for the fabricated PILF structure. Available broadband sources were too weak to directly measure this data. As in the last figure, the star represents the wavelength of a common communications laser, 1.319 μm . Significantly higher modulation could be achieved by shifting the transmission dip closer to this operating wavelength..... | 29 |
| Figure 19. Measured modulation at 1 kHz. This data was taken directly from an oscilloscope trace. The modulator was driven with a 10 V amplitude signal..... | 30 |
| Figure 20. Modulation at 10 MHz as measured on an RF spectrum analyzer. The driving signal was a 30 dBm sinusoidal signal. The signal-to-noise ratio is better than 70 dB. | 30 |
| Figure 21. Simplified fabrication procedure. The EO polymer film is deposited onto a quartz substrate and the polymer is then brought into contact with the half-coupler. UV epoxy or index matching fluid can be used to assure good optical contact. | 31 |
| Figure 22. Transmission spectrum of a PILF structure assembled using the procedure illustrated in Figure 21. The sharp, well defined dips indicate that good optical contact was achieved between the EO polymer and the half-coupler..... | 32 |
| Figure 23. Two tone intermodulation distortion. Even if working in less than an octave bandwidth, several terms fall within band and cannot be eliminated. It is these terms that ultimately limit the spurious free dynamic range..... | 33 |
| Figure 24. Output power vs. input power illustrating the relationship between the modulated signal (slope = 1), the second order terms (slope = 2), and the third order terms (slope = 3). | 34 |
| Figure 25. Measured (crosses) and theoretical fit (solid line) of the PILF structure. | 35 |
| Figure 26. Theoretical modulation as calculated from the fit shown in Figure 25..... | 36 |
| Figure 27. Calculated output power vs. input power, showing all spurious terms. From this plot, the SFDR can quickly be determined. | 36 |
| Figure 28. EO figures of merit for DR1 sidechain polyimide and an optimized polymer using chromophores of the new generation. A shift in absorption wavelength of 30 | |

nm has been assumed when going from solution into bulk polymer phase. Extrapolations to wavelengths closer than 100 nm to λ_{max} are not reliable since the two level model in this form is only valid outside of resonances. The dispersion for LiNbO_3 is given for comparison.....39

| | |
|-----------------------------------------------------------------------------------------------------------------------|----|
| Figure 29. Estimate of the resonantly enhanced modulation in a PILF device operated close to an absorption peak. | 40 |
| Figure 30. Variations of conformation-locked chromophores with enhanced nonlinearity and thermal stability..... | 43 |
| Figure 31. Chromophores with ring-locked polyene bridges..... | 44 |
| Figure 32. Post-functionalized polyquinoline..... | 46 |
| Figure 33. Pre-functionalized polyquinoline..... | 46 |
| Figure 34. PILF device fabricated on a silicon micromachined half-coupler..... | 50 |

1. Executive Summary

Optivision has completed a Phase I STTR project with the objective of developing highly active, electro-optic (EO) polymers tailored for use in in-line fiber photonic devices. The specific Phase I tasks were:

- Synthesize or obtain a quantity of "development" polymer.
- Develop suitable processing and characterization methodologies.
- Perform device level testing of EO polymers using a polymeric in-line fiber (PILF) structure.
- Identify suitable nonlinear optical (NLO) chromophores for resonantly enhanced EO polymers.
- Develop a synthesis strategy for novel highly active EO polymers to be produced during Phase II.
- Perform a high level design of a device to be built during the Phase II effort.

We have successfully completed all of these tasks. We have developed new EO polyquinoline materials specifically tailored for use in PILF structures and demonstrated the use of these polymers in actual PILF devices. The new polyquinolines incorporate chromophores with large $\mu\beta$ values and red shifted absorption peaks, resulting in polymers with EO coefficients of approximately 30 pm/V at a wavelength of 1.3 μm .

Dr. Alex Jen's group at Northeastern University was able to supply us with a suitable quantity of a guest-host polyquinoline for use in the development of processing and characterization techniques. The ability to obtain this material allowed us to proceed rapidly in the development of processing methods, fabrication techniques, and characterization procedures suitable for use with similar EO polyquinolines with enhanced EO responses.

We have developed processing, fabrication, and characterization techniques suitable for use with EO polyquinolines. The guest-host polyquinoline was used for the development of these techniques which should be fully compatible with future resonantly enhanced EO polyquinolines. The ability to develop these procedures with this relatively plentiful material before applying the procedures to the preparation of more exotic EO polyquinolines was a critical component of the Phase I effort and was crucial to the success of the project.

We have fabricated a working polyquinoline PILF amplitude modulator and demonstrated its performance. This device was demonstrated at frequencies up to 10 MHz and is capable

of operation at frequencies up to 250 MHz. The measured signal-to-noise ratio at 10 MHz was better than 70 dB.

We have identified and synthesized several NLO chromophores suitable for incorporation into future EO polyquinolines. These exhibit large $\mu\beta$ products, red-shifted absorption peaks, enhanced thermal stability, and resistance to *cis-trans* isomerization.

We have developed several synthesis strategies for the synthesis of the highly active, polyquinolines to be pursued under later efforts (Phase II or otherwise). We have developed synthesis schemes involving both pre- and post-functionalized polyquinolines which enable the incorporation of a wide range of chromophores.

We have fabricated and demonstrated a high dynamic range amplitude modulator based on the PILF structure. High dynamic range modulators are required for a number of Air Force applications, including RF links and phased array antenna systems. The unique properties of the PILF structure make it well suited for use in these applications.

During future efforts we will further develop and optimize the EO polyquinolines to provide for larger $\mu\beta$ values while maintaining the long term stability of the polymer. In addition, we will utilize a variety of different characterization tools to investigate the linear and nonlinear properties of the new EO polymers and further develop the PILF structure as a characterization tool ideally suited for long term testing of EO polymer photochemical and thermal stability. We strongly believe that the optimized resonantly enhanced EO polymers developed under these efforts will allow the development of practical PILF-based devices such as the optical modulator mentioned above.

2. Introduction

2.1 Project Scope

Improved electro-optic (EO) materials are critical for advanced photonic devices such as efficient high speed modulators, rapidly tunable filters for wavelength division multiplexing (WDM), and low switching voltage directional couplers for space division switching. Due to their outstanding cost and fabrication advantages, EO polymers are leading candidate materials for these applications. However, for EO polymers to be used as a replacement for lithium niobate in standard integrated optics devices such as Mach Zehnder modulators or directional coupler switches, it is necessary for the EO polymer to be stable for brief exposure to 250 °C, to have an EO coefficient of greater than 30 pm/V, and to have a loss of less than 1 dB/cm. Although there has been recent significant progress on improving the temperature stability of EO polymer materials [1-5] there is no presently available EO polymer material that comes close to simultaneously satisfying the high EO coefficient and low loss requirements. Prospects for development of such an EO polymer material in the near future are doubtful, as a major scientific breakthrough in nonlinear optical (NLO) chromophore structure/property relationships would be necessary to provide the necessary EO response with no or little resonance enhancement.

During this Phase I effort, a team consisting of Optivision and Northeastern University, with the University of California, Davis (UCD) as a key subcontractor, has pursued the development of EO polymer materials suitable for use in polymeric in-line fiber (PILF) devices. The PILF technology offers a solution to the dilemma currently facing EO polymers by *opening up a new region of parameter space for EO polymer materials development*. Traditional waveguide devices rely on propagation totally within the polymer waveguide, even in regions in which the index will never be modulated. In contrast, in PILF devices, interaction with the EO polymer takes place only in the region where index modulation is required. The remainder of the propagation through the device takes place in standard, low-loss optical fibers. The relatively short interaction region with the active material characteristic of PILF devices makes it possible to tolerate absorption losses in that material as high as 100 dB/cm and greatly relaxes the design requirements of EO polymers, allowing the use of materials with electronic transitions shifted towards longer wavelengths, thus yielding larger EO coefficients. In addition, the ability to tolerate this absorption opens up the possibility of using resonant enhancement to greatly boost the

achievable EO response. With resonant enhancement, EO coefficients in excess of 100 pm/V are possible. Finally, due to their simplicity, PILF devices provide an excellent means for straightforward device level testing of candidate EO polymer materials. Testing is simplified since polymeric buffer layers and channel waveguides are not required and long-term testing is facilitated by the self-aligned nature of the device.

2.2 Technical Objectives

The technical objectives of the Phase I effort and brief summaries of the work performed under each of those objectives are as follows:

- *Synthesize or obtain a quantity of "development" EO polymer.* Professor Alex Jen's group at Northeastern University was able to supply us with a sufficient quantity of guest-host polyquinoline material. We were able to use this material to develop out processing and characterization techniques while concentrating synthesis efforts on new materials.
- *Develop suitable processing and characterization methodology.* We have developed spin coating, electric field poling (corona, parallel plate, and in-plane), and liftoff film deposition techniques compatible with EO polyquinolines. In addition, we have utilized a variety of techniques to fully characterize the linear and nonlinear optical properties of these material.
- *Perform device level testing of EO polymers using a PILF structures.* We have successfully fabricated a PILF structure incorporating the EO polyquinoline. We have demonstrated operation up to a frequency of 10 MHz. This device is limited in operating speed only by its electrode design and is capable of modulation at 250 MHz.
- *Identify suitable nonlinear optical chromophores for resonantly-enhanced EO polymers.* We have identified and synthesized several new chromophores which will be suitable for use in PILF structures. These chromophores exhibit absorption peaks shifted towards longer wavelengths and large $\mu\beta$ products. In addition, these chromophores possess enhanced thermal stability and resistance to *cis-trans* isomerization.
- *Develop a synthesis strategy for novel highly active EO polymers to be produced during Phase II.* We have developed several unique synthesis strategies for the incorporation of these chromophores into sidechain polyquinolines. Both pre- and post-functionalized synthesis schemes have been developed.
- *Perform a high-level design of a PILF device to be built during Phase II.* We have identified enhanced linearity amplitude modulators as a device structure to be further pursued under a potential Phase II effort. Preliminary design work has been completed.

2.3 Report Organization

The remainder of the report is organized as follows. Section 3 presents a brief overview of the PILF structure and applications. Section 4 introduces polyquinoline and discusses the advantages of this material. Section 5 discusses the processing and characterization methodology and its application to polyquinoline materials. Section 6 covers the fabrication and testing of a polyquinoline PILF structure. Section 7 discusses the synthesis of novel NLO chromophores and the incorporation of those chromophores into polyquinolines. Section 8 contains conclusions and discusses possible future work.

3. Overview of Structure Architecture

A diagram of the polymeric in-line fiber (PILF) structure is shown in Figure 1. The PILF structure consists of a fiber half-coupler with a multimode waveguide overlay consisting of an EO polymer and a set of modulating electrodes. The fiber half-coupler consists of a glass block into which a curved slot is cut. A standard single-mode optical fiber is cemented into this slot and the entire assembly is polished down until the most of the fiber cladding is removed over a portion of the fiber. Thus, at the top surface of the block, access to the evanescent fields in the fiber is possible in the region where the cladding is removed. Fiber half-couplers can be obtained commercially for a fraction of the cost of fiber pigtailed integrated optics devices.

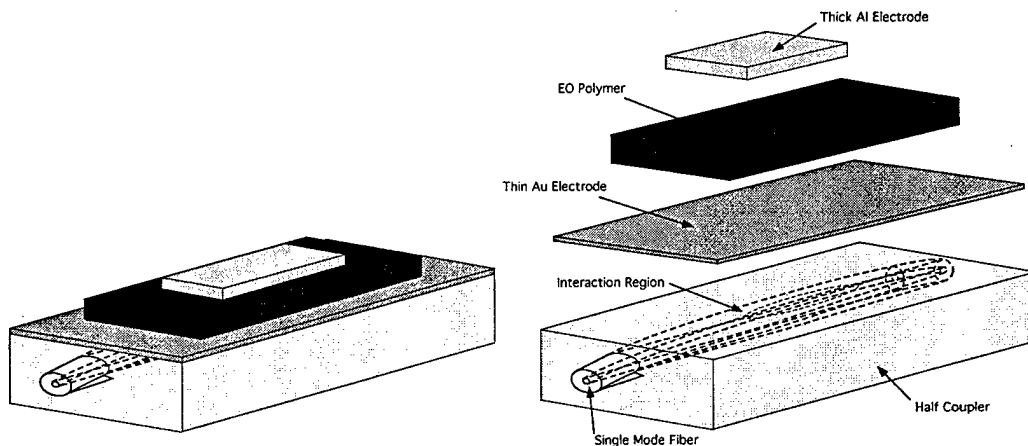


Figure 1. Polymeric in-line fiber (PILF) structure. The exploded view on the right clearly shows the curved fiber path and the interaction region where a portion of the fiber cladding is removed to gain access to the evanescent fields.

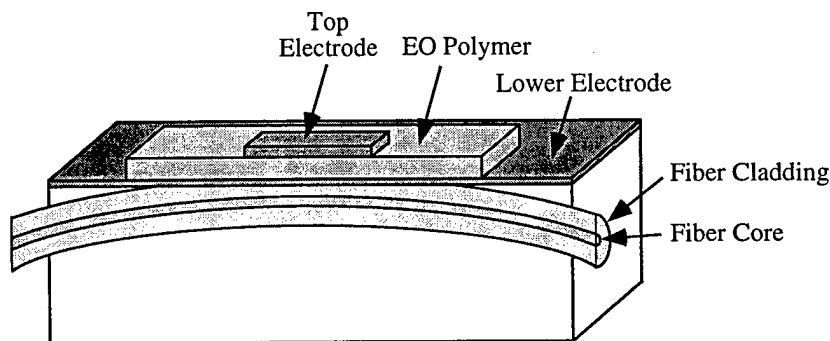


Figure 2. Cross section of the PILF structure shown in Figure 1.

Several different electrode structures are possible for control of the EO polymer waveguide overlay. These can general be summarized as lumped element geometries and coplanar geometries. A lumped element geometry, for our purposes, is a simple sandwich structure with electrodes located both above and below the EO polymer film. In the case of the PILF device, the lower electrode must be extremely thin (typically 10-15 nm if gold is used) in order to limit optical loss. With this electrode geometry, the applied control electric field and therefore the desired poling direction is normal to the surface of the film. In contrast, a coplanar electrode geometry has both electrodes in the same plane, either above or below the EO polymer film. The geometry allows the use of thick electrodes with the PILF structure because both electrodes are out of the optical path. The combination of thick electrodes, and a suitable coplanar electrode design, allows the development of extremely high speed devices.

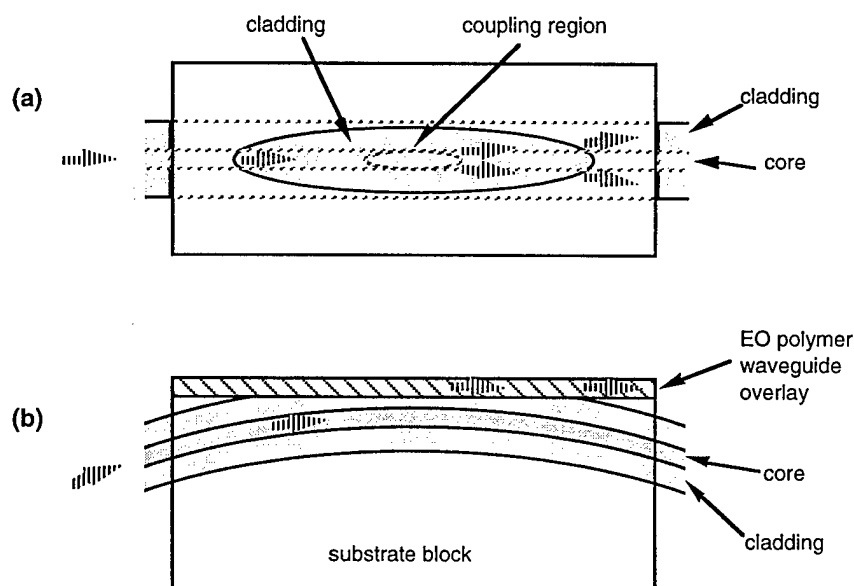


Figure 3. PILF device operation. A top view of the device is shown in (a) and illustrates the diffraction that occurs in the planar waveguide overlay. (b) shows a side view and represents the coupling from the embedded fiber into the waveguide overlay. For the sake of clarity, electrodes are omitted from both figures.

The operation of the PILF structure is based on the electro-optical control of the evanescent coupling from the embedded optical fiber to the polymer waveguide overlay (Figure 3). The transfer of optical power occurs in an "interaction region" which is determined by the radius of curvature of the fiber in the glass block -- a larger radius will result in a longer interaction region. The commercial devices we are currently using have an interaction

region approximately 1 mm long. Efficient optical power transfer occurs only for certain wavelengths of light that have the same effective index of refraction in the embedded fiber and the EO polymer waveguide overlay. Under certain conditions, the transfer of optical power is efficient enough to deplete the intensity of a narrow band of wavelengths centered around the exact phase matching wavelength. This results in a sharp, narrow dip in the optical fiber transmission spectrum with a center wavelength that can be electro-optically tuned, since the phase matching wavelength is a sensitive function of the EO polymer index of refraction. Figure 4 shows a representation of such a dip and illustrates the effects of voltage tuning the phase matching wavelength. Dips with attenuations of greater than 30 dB have routinely been achieved in our labs.

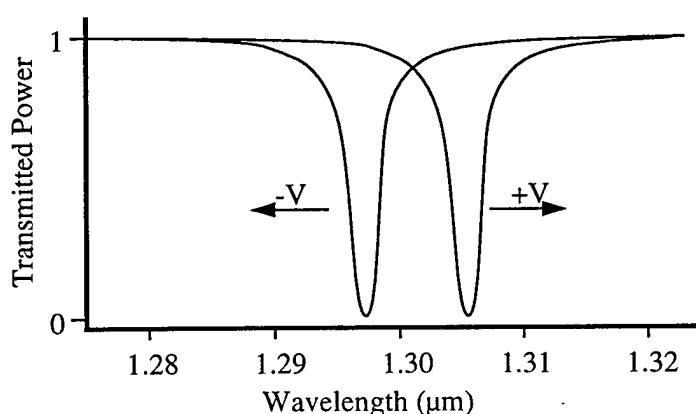


Figure 4. Representation of the transmission spectrum (transmitted power vs. wavelength) of a PILF structure illustrating the dip at the phase matching wavelength. The two curves represent the effect of voltage tuning the phase matched wavelength.

Clearly these PILF devices can be used either as modulators or as wavelength filters. Operation as an optical intensity modulator for a fixed wavelength narrow band laser source is readily achieved by biasing the modulator with a DC voltage to bring one edge of a transmission dip in coincidence with the laser wavelength and then superimposing the modulation signal on the DC bias voltage. The signal strength is proportional to the first derivative of the dip profile at the bias point. Operation as a wavelength filter is achieved simply by supplying sufficient DC control voltage to move the dip location to the wavelength of interest. Over 30 dB attenuation of light at the selected wavelength can be obtained. Discrimination between adjacent WDM channels depends on the dip width relative to the WDM channel spacing. The dip width is a function of the strength of the evanescent coupling and of the length of the interaction region. The PILF devices we have made so far have not been optimized for narrow band filter applications and have exhibited

typical dip widths on the order of 10 nm FWHM. Using optimized PILF filter designs with longer interaction regions and controlled evanescent coupling strength, it should be possible to achieve dip widths on the order of the 50 - 100 GHz (0.4 - 0.8 nm) channel spacing desired for many WDM applications.

It is important to note that for the PILF modulator device, due to the short interaction region and because only the light that is coupled out of the fiber propagates in the EO polymer overlayer, absorption coefficients of over 100 dB/cm can be tolerated in the EO polymer materials. This enables the use of EO polymers with strong resonant enhancement of the EO coefficients. This is in sharp contrast to traditional waveguide devices such as Mach-Zehnder modulators. In those devices, the light propagates within the EO polymer for the entire length of the device, including passive regions. For that reason, material loss requirements in devices such as Mach-Zehnder modulators are extremely stringent and resonant enhancement cannot be utilized.

4. Electro-Optic Polyquinolines

This section introduces the polymer system that we have chosen as a focus for this research effort. We briefly discuss the material and its advantages, relative to polyimides. The material structure is also introduced. More detailed analysis of the chromophore synthesis and of the material characterization will appear in later sections.

The polymer we selected for study under this effort was polyquinoline. We chose to pursue the development of this polymer for a number of reasons. When compared to polyimides, polyquinolines are a much "under-investigated" family of polymers. Therefore, the commercial availability of their starting monomers is quite limited. However, they appear to have a unique combination of properties which suggest their good potential for use in high performance NLO polymers. From a large array of published structures, it is clear the physical properties of polyquinoline can be fine-tuned by a suitable choice of the linking groups,. In particular, these linking groups can enhance solubility while maintaining or improving thermal stability, thus allowing the realization of polymers which are viable candidates for use in high performance EO devices. A major distinction between polyquinolines and polyimides is that while polyimides are usually processed through a polyamic acid pre-polymer and then subsequently cyclized to the polyimide, soluble polyquinolines are processed as fully cyclized polymers, and therefore require no post-cure.

Polyquinolines offer numerous advantages over other polymer systems such as:

- Very low dielectric constant: (2.6 - 2.8)
- Very low moisture uptake: (0.1 - 0.15%) (superior when compared to polyimides)
- Stable in solution at room temperature (Not as sensitive as polyamic acids)
- Very high glass-transition temperatures (250-400°C) and thermal stability (> 450 °C)
- Low shrinkage

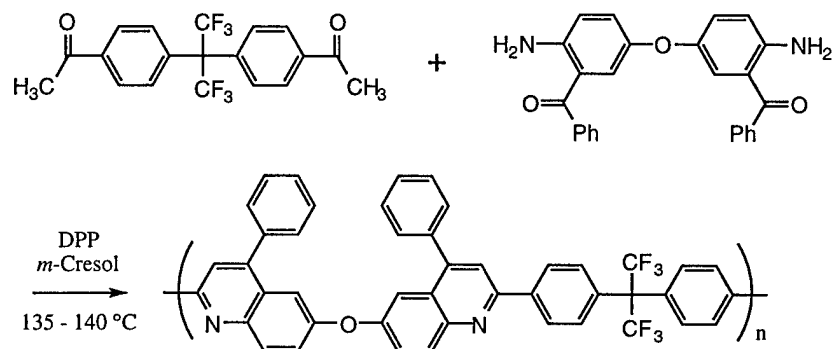


Figure 5. Chemical synthesis of fluorinated polyquinoline.

By taking advantage of the ease of formulation, Dr. Jen's group has demonstrated that very good optical quality NLO polymer thin films can be deposited onto conducting glass or silicon substrates using standard spin coating techniques. These films can also be heated and poled at high temperatures without damage.

Since the PILF structure only requires a single layer of active EO polymer, the stringent mechanical property requirements for EO polymers, which are required to sustain the overcoating of cladding polymers, are greatly relaxed. It is possible to take advantage of the easy formulation of the guest/host polyquinolines to incorporate a series of very active NLO chromophores with $\mu\beta$ values ranging from 6,000-13,000 $\times 10^{-48}$ esu (measured at 1.9 μm using EFISH) to achieve very large r_{33} values.

The following sections will go into greater detail in describing the chromophores that we have incorporated into the polyquinoline-based polymers and the characterization of those materials. In addition, we will describe the development of fabrication procedures compatible with polyquinoline and the fabrication of PILF structures incorporating this material.

5. Processing and Characterization Methodology

In this section we will discuss the approach used to develop the processing and characterization techniques required for use with the polyquinoline materials under development. These techniques will later be used for the fabrication of PILF devices, as described in Section 6.

5.1 Guest-Host Polyquinoline

One of the key goals of the Phase I effort was to identify and obtain a quantity of "development" polymer. This was to be a material that would be chemically similar to the proposed polyquinolines under development. The availability of this material would allow processing and characterization techniques to be developed in parallel with the actual development of the EO polyquinolines.

The material that we identified is shown in Figure 6 and was supplied to Optivision by Alex Jen's group at Northeastern University. This material is a guest-host polyquinoline mixture with a highly active chromophore ($\mu\beta = 6,200 \times 10^{-48}$ esu) and a relatively high doping density (25 % by weight). The glass transition temperature (T_g) is approximately 165 °C for the guest-host mixture, compared to 265 °C for the neat polyquinoline.

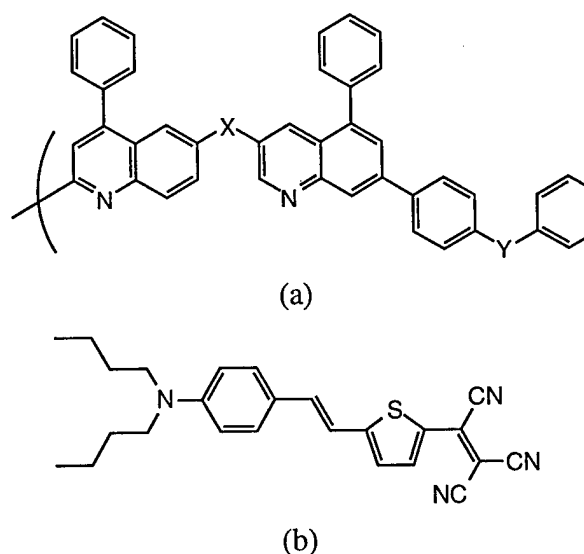


Figure 6. Chemical structure of both the (a) polyquinoline host and (b) dibutylaminobenzene-thiophene stilbene tricyanovinyl guest of the mixture that was used as a "development" polymer. The chromophore concentration was 25 % by weight.

5.2 Processing and Characterization

The guest-host mixture was dissolved in cyclopentanone and filtered through a 0.2 μm filter. Thin films of the polymer could then be prepared using standard spin coating techniques. Films were then dried in a vacuum oven at temperatures well below the glass transition temperature to avoid any problems with chromophore evaporation. Samples were poled with a relatively conventional corona poling setup which used a 2.5 cm long thin tungsten wire held 1 cm above the polymer surface as the corona electrode.

5.2.1 Linear Optical Properties

In order to accurately model the PILF structure, we required accurate measurements of the optical properties of all the materials involved. These were, of course, well known for the optical fiber (core and cladding) and the metal layers but the properties of the EO polymer had to be measured directly. This was done by preparing a thin film on a silicon substrate and measuring the properties of that film with a spectroscopic ellipsometer. This allowed the determination of both the ordinary and extraordinary refractive indices over the wavelength range of interest. The results are shown in Figure 7. In addition, another sample was prepared on a glass slide in order to measure the absorption. This was done with a conventional spectrophotometer and the results are shown in Figure 8. Because of the birefringence of this material, it was not possible to determine the imaginary part of the refractive index directly from the spectroscopic ellipsometer measurement.

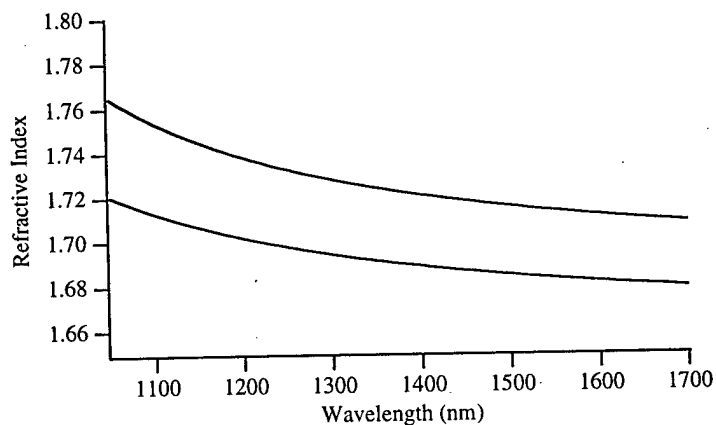


Figure 7. Refractive indices of the guest-host polymer as measured by spectroscopic ellipsometry. The upper curve is the extraordinary index while the lower curve is the ordinary index

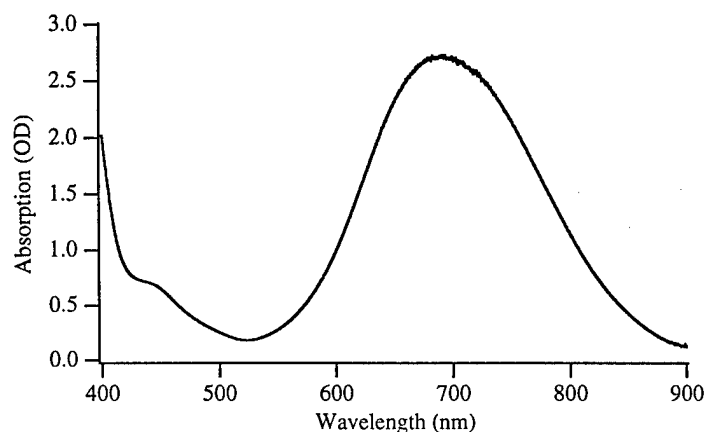


Figure 8. Absorption spectrum of the polyquinoline guest-host normalized to a 1 μm film thickness. The absorption peak is significantly red-shifted and located at approximately 690 nm.

5.2.2 Nonlinear Optical Properties

Numerous methods exist to quantify the nonlinear optical properties of EO polymers. Mach-Zehnder interferometry [6] and polarimetry [7] have been used to extract the Pockels (EO) coefficients. These methods are easy to implement and suitable for dispersive measurements of the EO coefficients, r_{13} and r_{33} . Their major drawbacks are that: a) the EO coefficients cannot be extracted independently (a ratio must be assumed); b) the refractive indices have to be measured independently (necessary to accurately calculate the EO coefficients and by itself a difficult task at the level of required accuracy); and c) these methods ignore multiple reflection effects in stratified samples. André Knoesen's group at the University of California, Davis, has developed a measurement method that does not share these drawbacks and is easily performed at multiple wavelengths [8]. The method is based on reflectance vs. angle of incidence scans of an asymmetric Fabry-Perot structure consisting of a metal/EO polymer/metal sandwich.

Fabry-Perot samples utilizing the guest-host polyquinoline were prepared with a liftoff deposition procedure, described fully in Section 6.2. To prepare the nonlinear films, the EO polyquinoline was spin coated onto glass-PAA (poly(acrylic acid)) donor substrates and dried under vacuum at a temperature of 80 $^{\circ}\text{C}$. Following corona poling at a temperature of 163 $^{\circ}\text{C}$, films were lifted off and deposited onto glass substrates previously coated with a 200 nm thick gold layer. The deposited polyquinoline film had a thickness of 4.3 μm . A partially reflecting upper electrode (23 nm thick) were then deposited by e-beam evaporation.

The reflectance and modulated reflectance characteristics were determined with the experimental configuration shown in Figure 9.

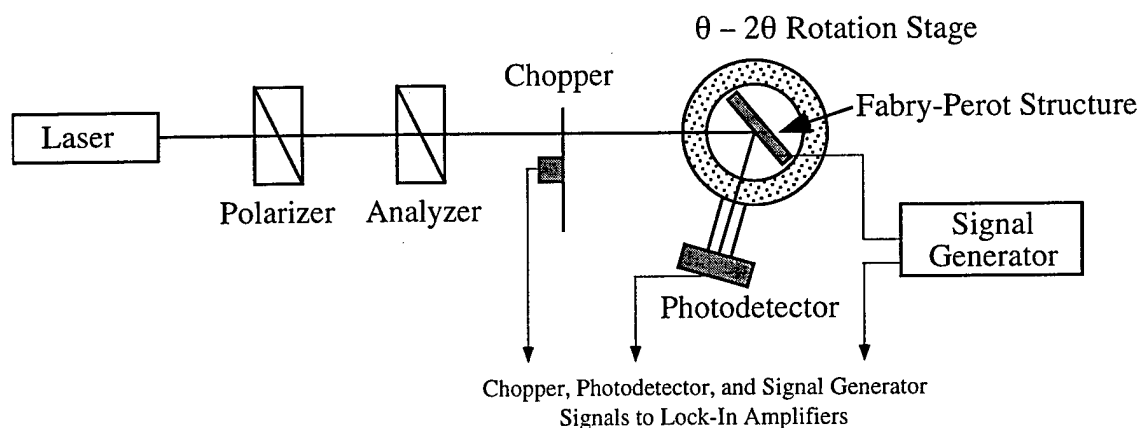


Figure 9. Experimental configuration for the dispersive measurement of the Pockels coefficient using a Fabry-Perot reflection modulator. The photodetector signal is sent to two separate lock-in amplifiers. The sync signal from the chopper is sent to one lock-in to detect the intensity of the light reflected from the Fabry-Perot structure. The sync signal of the signal generator is sent to the other lock-in to detect the light modulated by the Fabry-Perot structure

Reflectance and modulated reflectance measurements were taken as a function of the angle of incidence. The polarizer was set at 45° to ensure that after the analyzer equal intensities of TE (s) and TM (p) polarized light were incident onto the device. The device was positioned by a stepper motor θ - 2θ rotation stage. A low noise silicon photodiode receiver was used for detection and both the reflected and modulated reflected intensities were detected synchronously. Two lock-in amplifiers were used, one for the reflectance and the other for modulated reflectance measurements. The reflected intensity was calculated from the detection of the first fundamental spectral component of the squarewave modulated intensity that resulted from mechanically chopping the incident beam at 370 Hz. The modulated reflected intensity was detected from the sinewave modulated intensity that resulted from electro-optically modulating the refractive index of the EO polymer with a 15 V amplitude, 1 kHz sinusoidal signal. The sample orientation and data acquisition were under computer control.

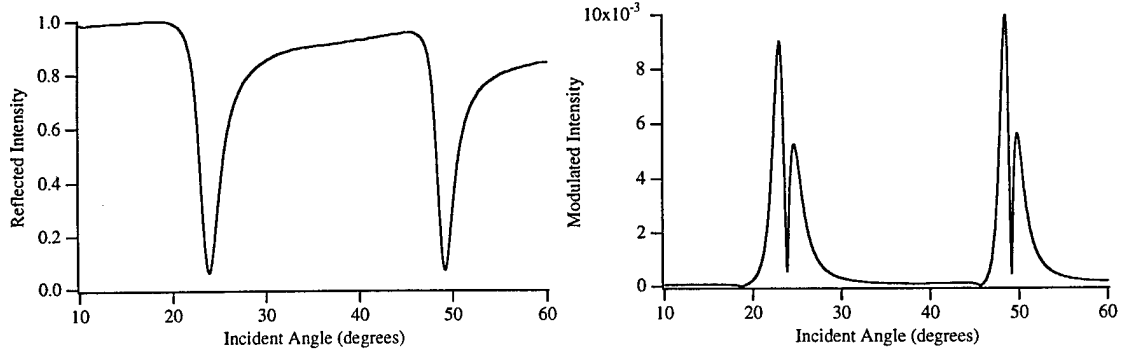


Figure 10. Reflected and modulated intensities measured with the Fabry-Perot structure at 1.064 μm (TM polarization shown, TE is similar).

The steps followed to extract the refractive indices and Pockels coefficients are described next. An electromagnetic plane-wave analysis [9,10] is used to model the structure and From the experimental scans for the TM and TE polarizations the extraordinary, n_E , and ordinary, n_o , refractive indices are respectively fitted to an electromagnetic plane-wave analysis. This analysis was implemented in MATLAB [11] and allows rapid, accurate modeling of the entire structure, including the metal electrodes, and allows the use of spectroscopic data for the indices of all materials. The fitting routine is a Levenberg-Marquardt nonlinear least-squares algorithm. Knowing the linear parameters we proceed to extract the r_{13} and r_{33} coefficients by fitting them to the modulated reflectance vs. angle of incidence scans. The EO coefficients, r_{13} and r_{33} , are independently extracted; the TE scan yields the r_{13} coefficient and the TM scans yields the r_{33} coefficient. This method is capable of performing dispersive measurements of the linear and nonlinear parameters and, if necessary, can operate with an incoherent light source so that the characterization is possible at most wavelengths. Table 1 summarizes the extracted linear and nonlinear constants obtained from the TE and TM scans for a wavelength of 1.064 μm .

Table 1. Regression analysis results for TE and TM polarizations ($\lambda = 1.064 \mu\text{m}$).

| | TE | TM |
|------------|----------------------------------|----------------------------------|
| n_o, k_o | $1.737 - j 6.058 \times 10^{-4}$ | -- |
| n_e, k_e | -- | $1.746 - j 2.954 \times 10^{-3}$ |
| r_{13} | 7.33 pm/V | -- |
| r_{33} | -- | 26.4 pm/V |

5.2.3 Temporal Stability

Although this material was a guest-host with only a moderate glass transition temperature, we nonetheless were interested in determining the long term temporal stability of a poled sample. This was done by heating a poled sample to 80 °C and measuring the EO coefficient over a long period of time. As expected, a relatively fast initial decay was noted but after approximately 100 hours, the decay leveled off. The retained EO coefficient, approximately 62 % of the initial value, was maintained for over 1000 hours at the elevated temperature. The results are shown in Figure 11.

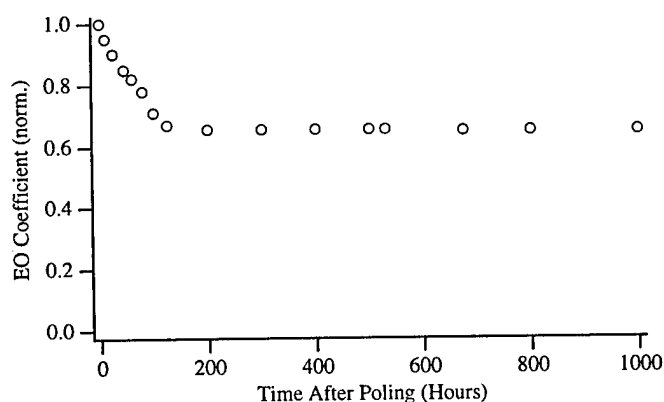


Figure 11. Temporal stability of the guest-host mixture at a temperature of 80 °C. After an initial decay, the measure EO coefficient was stable for more than 1000 hours.

Although the initial decay of the electro-optic activity was quite large, it must be remembered that this is a guest-host material intended primarily for the development of fabrication and characterization procedures. Functionalized polymers, which would be

required for use in commercial devices, would have higher glass-transition temperatures and better temporal stability.

5.2.4 Thermal Conductivity

While fabricating and characterizing the polyquinoline samples, we had noticed some discrepancies in the values of measured EO coefficients. In the techniques reported here, an r_{33} of 26.4 pm/V at 1.064 μm was measured. However, in a previous measurement, Dr. Jen's group had measured 29 pm/V at 1.3 μm . While these values were similar, the measurement at the shorter wavelength should have been significantly larger due to resonant enhancement of the nonlinearities. We determined that the discrepancy was due to the sensitivity of this material to the poling temperature.

In order to determine an appropriate poling temperature, we investigated the resistivity and conductivity of the guest-host polyquinoline. The results of those measurements are illustrated in Figure 12. These measurements indicated that a temperature of approximately 160 °C would be suitable for poling. In addition, we performed *in situ* measurements of the generated second harmonic as a function of temperature from a sample during poling and depoling. The poling current as a function of temperature was also measured. The heating rate was 2.5 °C per minute. These results are shown in Figure 13 and indicate that a maximum generated second harmonic signal is achieved at approximately 130 °C, significantly below the 160 °C predicted by the data of Figure 12 and the measured glass transition temperature of 165 °C.

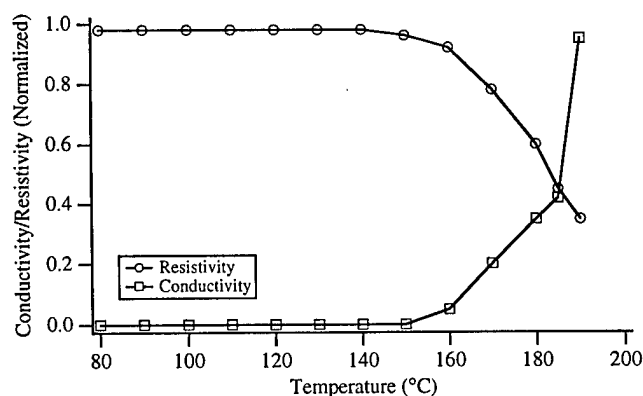


Figure 12. Resistivity and Conductivity of the polyquinoline guest-host polymer.

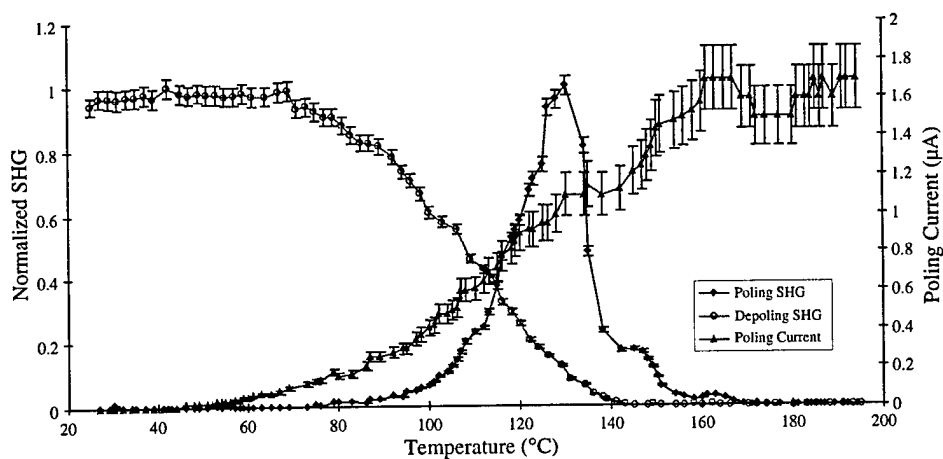


Figure 13. Measured second harmonic signal vs. temperature during both poling (field applied) and depoling (no field applied). Also shown is the poling current as a function of temperature.

This discrepancy in poling temperatures may be explained by the nature of a guest-host system. Because the chromophores are not securely attached to the polymer backbone, orientation is possible at temperatures below the glass transition temperature. In addition, at higher temperatures, as the conductivity of the polymer increases, the poling field decreases and the orientational forces on the chromophores therefore also decrease. And finally, the thermal randomization forces are also greater at elevated temperatures.

6. PILF Structure Fabrication and Evaluation

In addition to the development of processing and characterization methodology, the relatively large quantity of the EO polyquinoline allowed us to develop procedures for the fabrication of PILF test structures including a working amplitude modulator. In this section we will present various design and fabrication aspects associated with PILF structure fabrication. We will also present test results from completed structures showing their use as optical modulators.

6.1 Structure Modeling

In order to fabricate a structure capable of operating at a desired wavelength, it is first necessary to model the structure to determine the appropriate EO polymer film thickness. As previously mentioned, the operating wavelength is determined by a phase match between the fiber mode and the mode in the polymer waveguide overlay. The effective index of the fiber mode is determined by the fiber parameters, leaving as the only variable the thickness of the waveguide overlay.

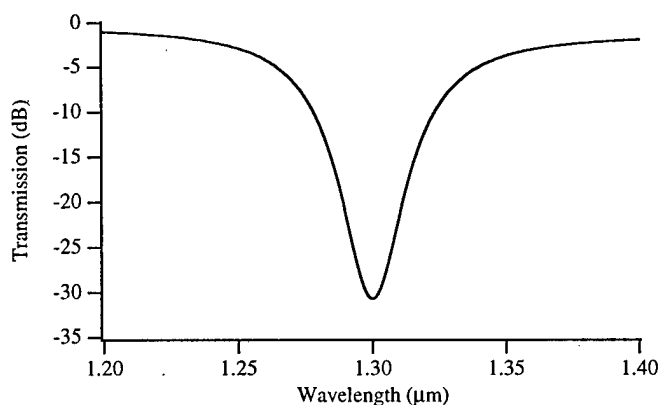


Figure 14. Simulation of the transmission through a PILF structure fabricated with standard half-coupler, a 10 nm gold lower electrode, a 2.03 μm thick polyquinoline layer, and a 200 nm thick aluminum upper electrode. These design parameters result in phase matching at a wavelength of 1.3 μm .

We have used an electromagnetic plane-wave analysis similar to that used to model the asymmetric Fabry-Perot structure [9,10] that takes into account the anisotropy associated with EO polymers to model this structure. This analysis was once again implemented in MATLAB and allows the use of spectroscopic data for the indices of all materials (fiber,

electrodes, EO polymer). Once the refractive indices for each layer have been determined, typically by spectroscopic ellipsometry, the performance of the PILF structure can be simulated. The EO polymer waveguide overlay thickness can then be varied to obtain a phase match, and a corresponding transmission dip, at the desired wavelength. The results of such a simulation are shown in Figure 14.

The simulation in Figure 14 shows the transmission spectrum of a PILF structure with a 10 nm thick gold lower electrode, a 2.03 μm thick polyquinoline layer, and a 200 nm thick aluminum upper electrode. Following simulation, these device parameters were used as guidelines for the fabrication of the preliminary PILF structures.

6.2 Liftoff Deposition of EO polymer film

The common techniques employed to fabricate EO polymer devices and structures involve spin coating of a EO polymer layer and vacuum deposition of metal electrodes [8,12,13]. In order to realize second-order nonlinear effects, the EO polymer must then be poled. This involves heating the EO polymer and underlying substrate and applying a large electrostatic field to align the NLO chromophores. In some cases, one or more of these processing steps may lead to damage of the underlying substrate, and therefore impose restriction on device configurations. For example, poling fields have the potential to damage underlying circuitry and, more importantly for our case, spin coating can damage substrates such as half-couplers. We have developed a processing technique which allows high quality films to be selectively deposited onto substrates without direct spin coating [14,15]. This deposition procedure has an added benefit in that it allows the fabrication of corona poled EO polymer devices on a variety of substrates. While similar techniques have been demonstrated for the fabrication of structures for quasi-phase matched second harmonic generation, our technique is directly applicable to the selective deposition of EO polymer layers for use in EO devices and addresses such issues as adhesion at metal-EO polymer interfaces. The technique involves the deposition of the EO polymer onto a temporary substrate which is treated with a "release layer". Following deposition and corona poling, the EO polymer film is cut to the desired final size and released from the temporary substrate. The prepared and poled EO polymer film is then deposited onto the final substrate and can be easily integrated into an EO device structure. This technique allows the deposition of the EO polymer to be confined to the region of interest and allows the thickness of the film to be determined prior to deposition on the final substrate. In addition, multiple films of identical thickness can be deposited in multiple locations or onto

different devices. This thickness control is crucial for the repeatable fabrication of devices which rely on control of optical resonances, such as the PILF structure.

The fabrication of a typical PILF structure utilizing the liftoff deposition technique is shown schematically in Figure 15. The structure is fabricated by spin coating and drying a 1 μm thick poly(acrylic acid) (PAA) release layer onto a glass slide. A layer of EO polymer is then spin coated onto the PAA layer and corona poled. Following poling, a small metal electrode is deposited onto the EO polymer by e-beam evaporation. The dimensions of this electrode are typically controlled by shadow masking. The EO polymer/aluminum structure is then cut into small sections and freed from the substrate by dissolving the PAA layer in water. The sections are then deposited onto a half-coupler onto which has previously been e-beam evaporated a thin gold lower electrode. In order to assist in deposition and repositioning of the EO polymer layer, a surface treatment consisting of 3-mercaptopropionic acid in ethanol is applied to the lower gold electrode prior to the deposition of the EO polymer. This surface treatment allows the residual water to wet the surface of the gold, thus allowing the EO polymer film to be easily repositioned and enabling the film to dry without buckling. Following positioning of the EO polymer/aluminum structure, the excess water is removed and the completed structure is allowed to air dry. The final structure consists of a fiber half-coupler, a thin gold lower electrode, an EO polymer layer, and a thick upper electrode (typically gold or aluminum). The adhesion of the EO polymer to the lower gold electrode is typically sufficient to withstand attempted removal via Scotch tape placed on top of the structure.

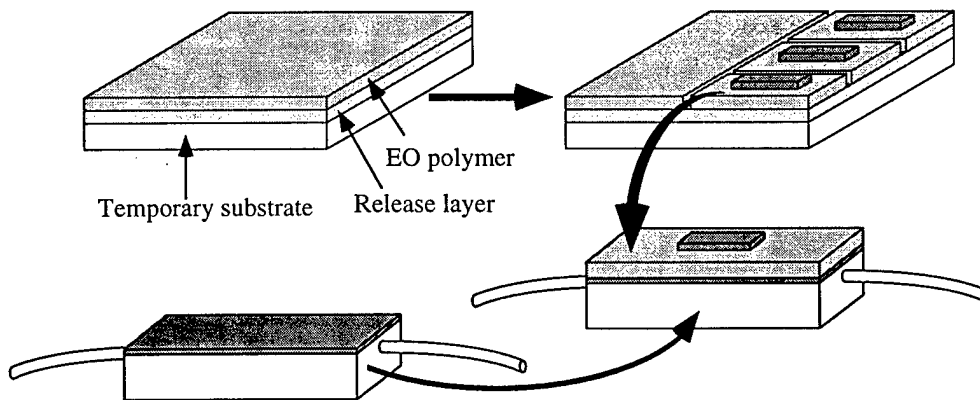


Figure 15. Liftoff deposition technique for the preparation of PILF structures. The EO polymer film is completely prepared, including poling and deposition of metal electrodes, on a temporary substrate and then transferred to the half-coupler block.

6.3 PILF Structure Fabrication

The fabrication of a PILF structure is fairly straightforward, as described in the previous section, and involves relatively few fabrication steps. Unlike conventional polymeric waveguide devices, the PILF structure does not require any channel waveguides or buffer layers.

The actual fabrication of a test structure was performed jointly by UC Davis and Optivision. A film of the EO polyquinoline was prepared by spin coating onto a glass-PAA donor substrate and drying under vacuum for 1 hour at a temperature of 80 °C. The glass-PAA donor substrate had previously been prepared by spin coating a 12.5 % by wt. solution of PAA (avg. $M_w = 90,000$), at 1500 rpm onto 1 mm thick glass slides and drying under vacuum for 1 hour at a temperature of 65 °C. Following deposition of the EO polymer film, the film was poled using standard corona poling techniques. The temperature was ramped to 170 °C and held at that temperature for 2 minutes before being lowered to a poling temperature of 160 °C. Once the film was at a stable temperature of 160 °C, a corona voltage of approximately 6 kV field was applied to a thin, 2.5 cm long tungsten wire held 1 cm above the film surface. The corona current was approximately 4 μ A. After 15 minutes at 160 °C, the film was cooled to room temperature with the electric field applied. After poling, a top electrode was formed by evaporating a 0.8 mm wide, 2 mm long, 200 nm thick aluminum layer onto the top of the EO polymer film. The lower electrode was formed by evaporating a 0.5 nm thick titanium adhesion layer and a 10 nm thick gold layer onto the surface of the half-coupler. All metallic layers were deposited with an e-beam evaporator. A 1 cm x 5 mm section of EO polymer which included the top electrode was then deposited onto the half-coupler using the liftoff deposition procedure describe in Section 6.2.

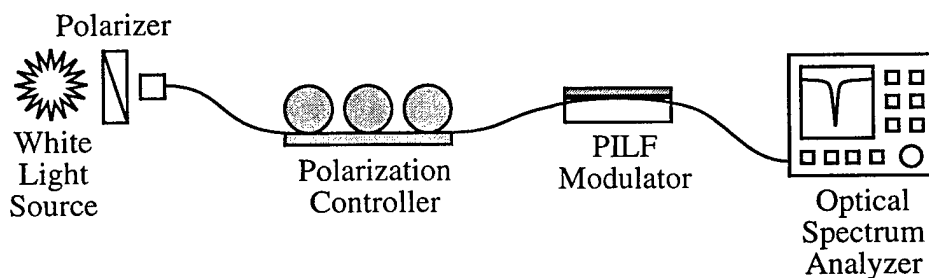


Figure 16. Experimental configuration used for preliminary evaluation of PILF modulator structures.

Preliminary testing of the completed PILF test structure was accomplished using the experimental configuration shown in Figure 16. In this configuration, a white light source is polarized and coupled into a single-mode optical fiber. Following a fiber polarization controller, the light is coupled into the PILF structure under test. The transmitted light is then detected using an optical spectrum analyzer. This test configuration allows the transmission dips to be evaluated, in terms of position, width, and depth. The results for the structure fabricated with the EO polyquinoline are shown in Figure 17. The solid line represents experimental data while the dashed line represents calculations based on the electromagnetic plane wave analysis. The figure shows a transmission dip that is better than 25 dB deep, centered at a wavelength of 1.23 μm . The data at bottom of the dip is noisy due to the low power of the white light source and the noise floor of the optical spectrum analyzer. The center wavelength of the dip indicates that the thickness of the polymer film used to fabricate this structure varied slightly from the thickness desired for operation at a wavelength 1.3 μm . Further profilometry measurements of the film and simulations of the structure confirmed that the thickness of the film used in this structure was approximately 1.89 μm . However, even though the device was not optimized for operation at 1.3 μm , it was still possible to measure amplitude modulation.

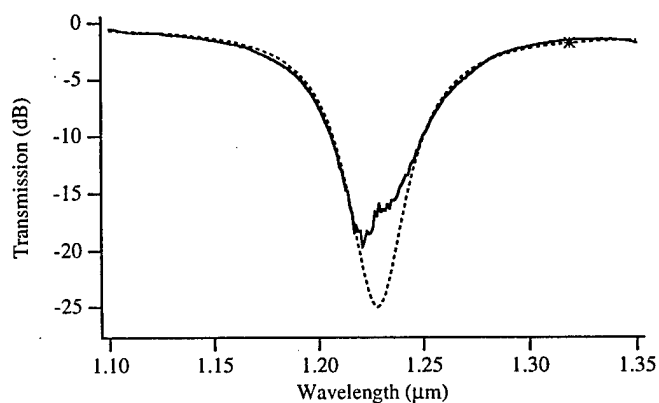


Figure 17. Transmission spectrum of the polyquinoline PILF structure. The solid line is the measured data while the dashed line is a theoretical fit. The discrepancy at low levels is due to the noise floor of the optical spectrum analyzer. The star represents the wavelength of a common communications laser, 1.319 μm .

Modulation was measured using a diode-pumped Nd:YAG operating at 1.319 μm . From the transmission spectrum shown in Figure 17, it can be seen that this wavelength is on the long-wavelength side of the transmission dip but the slope of the transmission spectrum at this wavelength is still nonzero. The observed modulation, defined as the change in transmission divided by transmission ($\Delta T/T$), was approximately 0.5 %. However,

referring to the simulation shown in Figure 18, we see that this operating point is somewhat removed from the optimum point and that we could expect approximately 16 % modulation with this drive voltage at the optimum bias point.

With an optimized device, it is easy to see how data such as that shown in Figure 17 and Figure 18 will allow the determination of the EO coefficients.

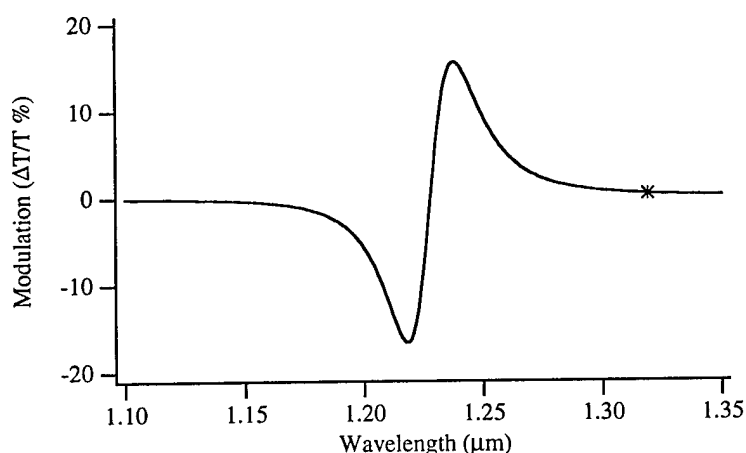


Figure 18. Theoretical modulation spectrum for the fabricated PILF structure. Available broadband sources were too weak to directly measure this data. As in the last figure, the star represents the wavelength of a common communications laser, 1.319 μm . Significantly higher modulation could be achieved by shifting the transmission dip closer to this operating wavelength.

Further testing demonstrating modulation was performed with a low frequency signal generator and a RF signal generator. A 10 V amplitude, 1 kHz sine wave was used to drive the PILF structure and the modulated light was detected with a New Focus 2011 detector. The detector output was then fed directly to an oscilloscope. An oscilloscope trace of the sine wave, illustrating clear detection of this signal, is shown in Figure 19. High speed modulation was achieved by driving the PILF structure with a RF signal generator providing +30 dBm at 10 MHz. The modulated light was detected using a New Focus 1611 detector and then fed to an HP 8593E microwave spectrum analyzer. A spectrum analyzer trace showing modulation at 10 MHz with a dynamic range of better than 70 dB is shown in Figure 20.

The fabrication and demonstration of this working PILF intensity modulator confirmed that the fabrication techniques we have developed are indeed compatible with the requirements of EO polyquinolines and are capable of enabling integration of those materials into

working devices. Although this was only a preliminary device, the fabrication procedures are fully compatible with optimized device structures and the electrode structure utilized has a 3 dB rolloff frequency of approximately 250 MHz (limited by the capacitance of the structure).

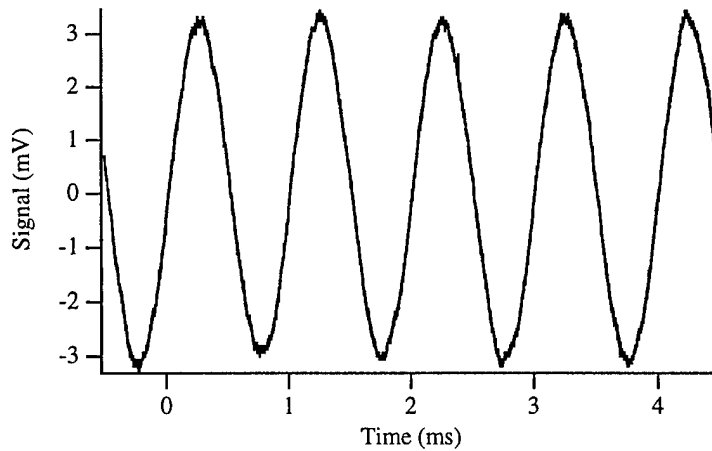


Figure 19. Measured modulation at 1 kHz. This data was taken directly from an oscilloscope trace. The modulator was driven with a 10 V amplitude signal.

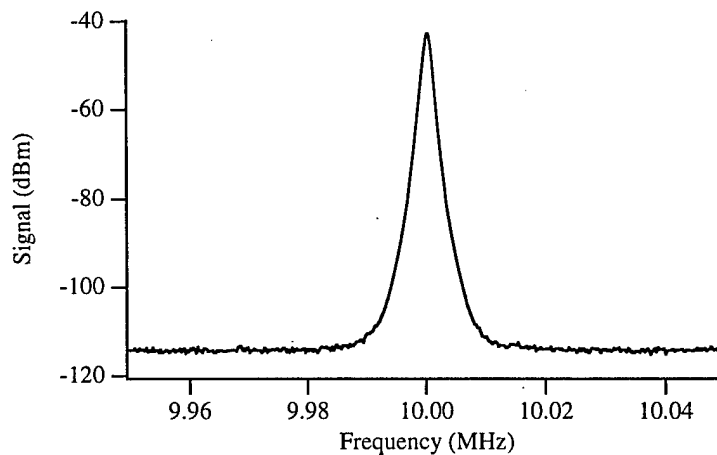


Figure 20. Modulation at 10 MHz as measured on an RF spectrum analyzer. The driving signal was a 30 dBm sinusoidal signal. The signal-to-noise ratio is better than 70 dB.

6.4 Modified Fabrication Procedure

Although the assembly of PILF structures using the liftoff deposition technique is not particularly difficult, we were interested in developing an alternative polymer deposition techniques which could eliminate the potentially troublesome release layer. One approach

that we have investigated and implemented is shown in Figure 21. In this technique, the EO polymer is spin coated using standard procedures directly onto a quartz substrate. Following drying and poling, the assembly is inverted and deposited directly onto the fiber half-coupler. A cross section of the assembled PILF structure is shown in Figure 21(b) and shows that, following assembly, the quartz substrate forms an overlayer on top of the polymer film. Quartz is required (as opposed to standard BK7 glass) due to its low index which is necessitated by the waveguiding conditions of the structure. A thin layer of UV epoxy or index matching fluid can be added between the half-coupler and the EO polymer film to assure optical contact. This assembly procedure eliminates several steps involved with the liftoff deposition technique and also allows easy reuse of the fiber half-couplers during characterization studies or device development. One additional advantage is that the use of the quartz overlayer results in a nearly symmetric waveguide overlay (quartz/polymer/fiber) as opposed to the traditional structure (air/polymer/fiber) and is therefore much less polarization dependent. Of course, the birefringence of the EO polymer and the difference in the two EO coefficients ultimately results in a polarization dependent device. However, the center wavelengths of the TE and TM dips are essentially identical, as opposed to that noted with the traditional structure, thus enabling the future development of a polarization insensitive device.

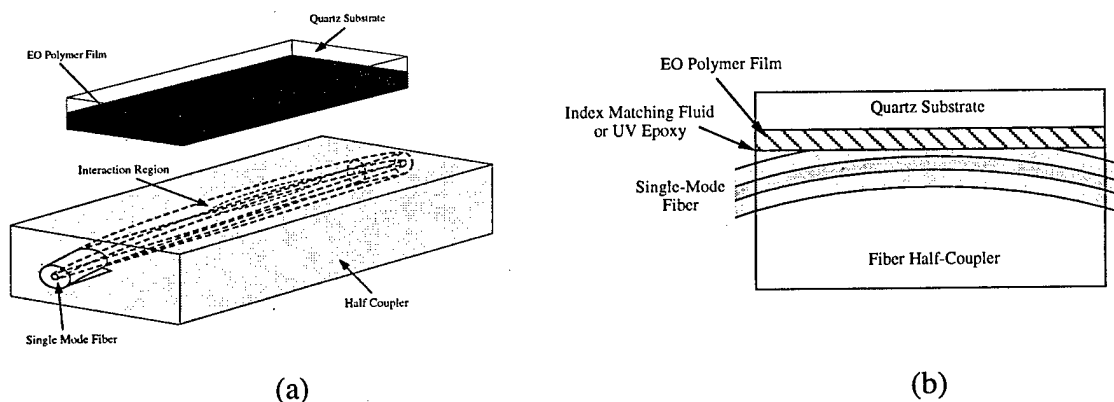


Figure 21. Simplified fabrication procedure. The EO polymer film is deposited onto a quartz substrate and the polymer is then brought into contact with the half-coupler. UV epoxy or index matching fluid can be used to assure good optical contact.

Figure 22 illustrates the transmission spectra of a PILF structure fabricated with this assembly technique which clearly shows deep dips -- indicative of strong coupling between the embedded fiber and the EO polymer film. This strong coupling could only occur if good optical contact between the two was obtained. We are still pursuing further

development of this fabrication technique and intend to use of for future development of PILF structures and devices.

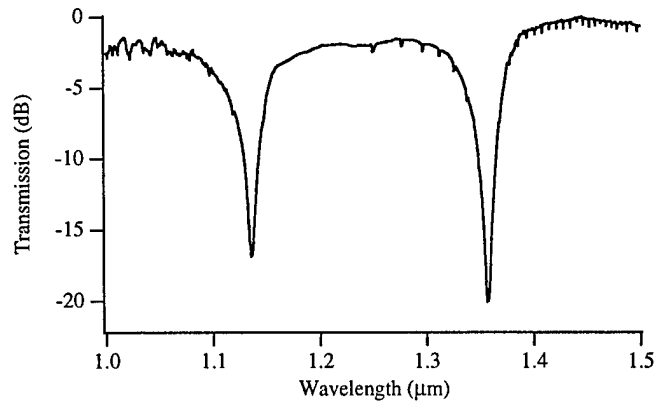


Figure 22. Transmission spectrum of a PILF structure assembled using the procedure illustrated in Figure 21. The sharp, well defined dips indicate that good optical contact was achieved between the EO polymer and the half-coupler.

6.5 PILF Spurious Free Dynamic Range

One of the particularly attractive applications for PILF devices is that of a linearized amplitude modulator. Linearized modulators are in great demand for a variety of high dynamic range applications, including RF links and photonically controlled phased array antennas. The primary limitation to modulator linearity is intermodulation distortion (IMD). IMD is caused when a two tone signal is input to a device and the nonlinearities of that device result in higher order terms which interfere with the desired signal. The most common interference comes from terms comprising $2\omega_1 - \omega_2$ and $2\omega_2 - \omega_1$ (where ω_1 and ω_2 are the frequencies of the input signals) (see Figure 23). Although it is possible for contributions to come from higher order terms, the majority of the IMD is proportional to the third derivative of the optical transfer function. A severe limitation of Mach-Zehnder devices is that the modulation (the first derivative of the optical transfer function) and the IMD (the third derivative) are both sinusoids and both directly related -- it is impossible to eliminate the IMD without eliminating the modulation. By contrast, in an asymmetric coupler device, such as the PILF structure, it is possible to engineer the optical transfer function (the transmission dip shown in previous plots) in order to obtain a large first derivative (modulation) and a small third derivative (IMD).

The characteristics of an externally-modulated high-dynamic-range analog EO link depend critically on the shape of the transfer function of the external modulator. Given the

modulator transfer function, we can expand the transmission versus voltage in a Taylor series about any chosen bias point and predict the intermodulation products and hence the spurious free dynamic range (SFDR), which is defined as the difference between the largest undistorted signal and the smallest detectable signal. Spurious signals corresponding to higher order terms of the Taylor series can fall in band and corrupt the desired signal. Figure 23 illustrates how third order terms can fall very close to the desired signal. It is often possible to eliminate many of the higher order terms simply by working with a relatively narrow bandwidth (an octave or less). However, as shown in Figure 23, once generated some spurious terms cannot be avoided.

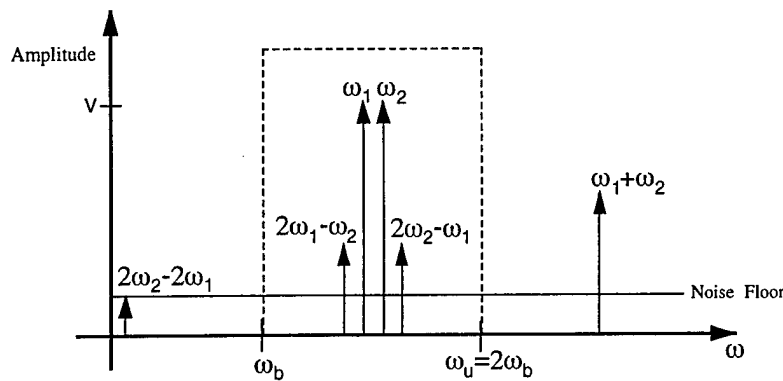


Figure 23. Two tone intermodulation distortion. Even if working in less than an octave bandwidth, several terms fall within band and cannot be eliminated. It is these terms that ultimately limit the spurious free dynamic range.

The Taylor series expansion of the transmission function of any device about the bias point is given by (showing only the first four terms):

$$T(V) = T_0 + V \left. \frac{\partial T}{\partial V} \right|_{V=0} + \frac{1}{2} V^2 \left. \frac{\partial^2 T}{\partial V^2} \right|_{V=0} + \frac{1}{6} V^3 \left. \frac{\partial^3 T}{\partial V^3} \right|_{V=0} + \frac{1}{24} V^4 \left. \frac{\partial^4 T}{\partial V^4} \right|_{V=0} \quad (1)$$

For a two-tone input, the substitution $V = V_1 \sin(\omega_1 t) + V_2 \sin(\omega_2 t)$ into Equation (1) allows the calculation of the compression of the fundamental signal and the spurious tones in the output. The highest amplitude tones for each of the powers of V are:

$$\begin{aligned}
T = T_0 &+ V_1 \sin(\omega_1 t) \left. \frac{\partial T}{\partial V} \right|_{V=0} + V_2 \sin(\omega_2 t) \left. \frac{\partial T}{\partial V} \right|_{V=0} + \frac{V_1 V_2}{2} \cos[(\omega_1 + \omega_2)t] \left. \frac{\partial^2 T}{\partial V^2} \right|_{V=0} \\
&+ \frac{V_1^2 V_2}{8} \sin[(2\omega_1 - \omega_2)t] \left. \frac{\partial^3 T}{\partial V^3} \right|_{V=0} + \frac{V_1 V_2^2}{8} \sin[(2\omega_2 - \omega_1)t] \left. \frac{\partial^3 T}{\partial V^3} \right|_{V=0} + \frac{V_1^2 V_2^2}{32} \cos(2\omega_2 - 2\omega_1 t) \left. \frac{\partial^4 T}{\partial V^4} \right|_{V=0}
\end{aligned} \tag{2}$$

Additionally there is a difference frequency term in the second order of equal amplitude to the sum frequency, and fourth order sum and difference frequency terms.

By expanding the Taylor series and calculating all of the spurious terms, it is possible to calculate the linearity of a particular modulator. This can be done by comparing the intensity of the desired linear modulation term to those of the various undesired spurious terms. Figure 24 represents one such comparison. This figure presents output power as a function of input power. At low powers, the only term detectable above the noise floor is the desired modulation signal. However, at higher powers other higher order terms rise above the noise floor and eventually dominate the detected signal. From the figure, it is easy to see that the SFDR is maximized at the point at which the spurious term is just equal to the noise floor, and therefore still undetectable.

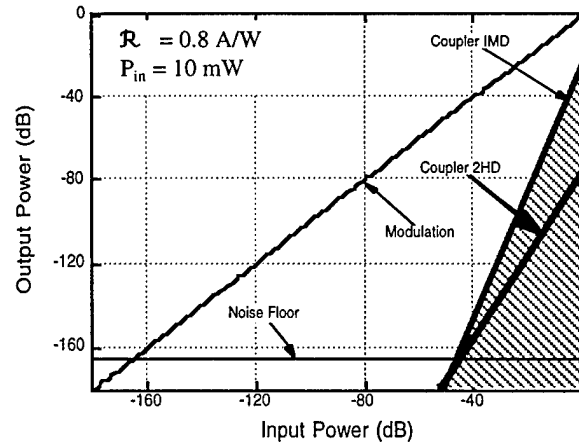


Figure 24. Output power vs. input power illustrating the relationship between the modulated signal (slope = 1), the second order terms (slope = 2), and the third order terms (slope = 3).

We have performed an analysis on the polyquinoline PILF modulator to evaluate its SFDR. A fit was generated by modeling the structure as an asymmetric coupler with loss in one of the guides. By modeling the device in this manner, the well known coupled waveguide

equations can be used to predict its behavior. Those coupled waveguide equations are given by:

$$\begin{aligned}\frac{\partial}{\partial z} A_1(z) &= -i\kappa A_2(z) \exp[i\Delta\beta z] \\ \frac{\partial}{\partial z} A_2(z) &= -i\kappa^* A_1(z) \exp[i\Delta\beta z] - \alpha A_2(z)\end{aligned}\quad (3)$$

where A_1 is the amplitude in the fiber, A_2 is the amplitude in the polymer, κ is the coupling coefficient, $\Delta\beta$ is the difference in propagation constants, and α is the loss in the polymer waveguide. The solution for the amplitude in the fiber, with the initial conditions $A_1(0) = 1$ and $A_2(0) = 0$ is:

$$A_1(z) = \frac{\exp[-z(\alpha - i\Delta\beta)/2] \{ (\alpha - i\Delta\beta) \sinh[zK_R/2] + \cosh[zK_R/2] K_R \}}{K_R} \quad (4)$$

The measured data and the fit using the asymmetric coupled waveguide model is shown in Figure 25.

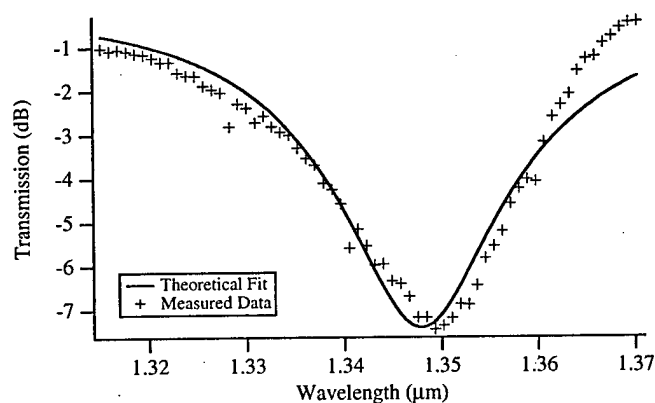


Figure 25. Measured (crosses) and theoretical fit (solid line) of the PILF structure.

Once the fit is obtained, it is possible to further simplify it by fitting it to a polynomial and then performing a Taylor series expansion on that polynomial. The Taylor series term corresponding to the first derivative is the desired modulation (see Figure 26), all other terms contribute spurious terms, both out of band and within the frequency band of interest.

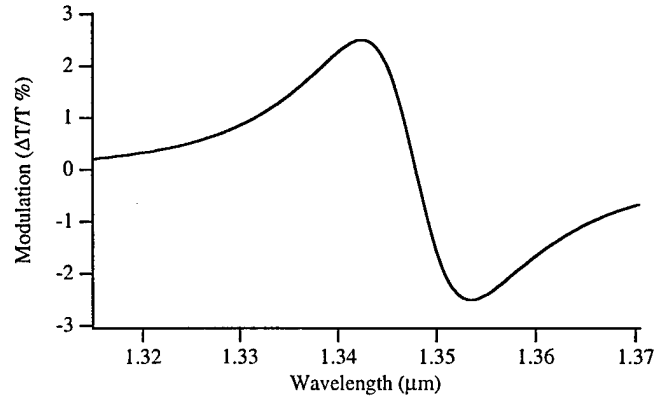


Figure 26. Theoretical modulation as calculated from the fit shown in Figure 25.

By including sufficient Taylor series terms to accurately approximate the fit to the measured data, we can accurately predict the SFDR performance of the device. In our case, we used a Taylor series with 35 terms. Figure 27 illustrates the relationships between the desired modulation and the higher order interference terms. The modulation is proportional to the first derivative of the transfer function and therefore has a slope of one (until it rolls off at higher powers). Second harmonic terms have slopes equal to two and third order IMD terms have slopes equal to four. The slopes shown in Figure 27 are not as simple due to contributions from higher order terms.

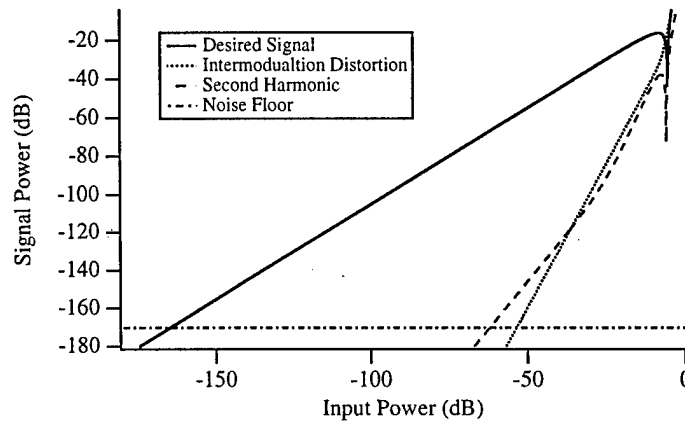


Figure 27. Calculated output power vs. input power, showing all spurious terms. From this plot, the SFDR can quickly be determined.

From the plot shown in Figure 27, the SFDR can be easily calculated. In this case, the SFDR is equal to $116 \text{ dB} \cdot \text{Hz}^{2/3}$ when limited by the third order IMD and $103 \text{ dB} \cdot \text{Hz}^{1/2}$ when limited by the second harmonic. Many applications utilize an octave bandwidth or less, and therefore the second harmonic falls out of band. In these cases the larger, IMD

limited value is used. Typical IMD limited numbers reported by standard Mach-Zehnder devices are on the order of $108 \text{ dB}\cdot\text{Hz}^{2/3}$ while some complex, and often bandwidth limited, linearization schemes have achieved values greater than $120 \text{ dB}\cdot\text{Hz}^{2/3}$. The numbers reported for this PILF structure represent a non-optimized device -- it is still possible to tailor the transmission spectra in order to achieve a considerably higher SFDR. To put these numbers in perspective, an increase in dynamic range of 10 dB will allow the range of a radar system to be increased 1.8 times.

7. Synthesis of Highly Active Electro-Optic Polymers

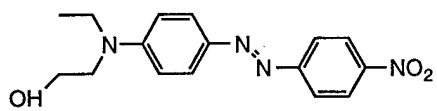
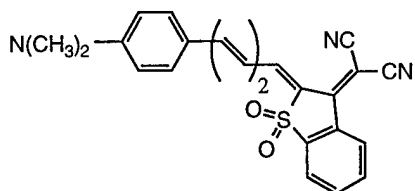
The overall objective of the material effort in this Phase I program is to develop new highly active EO polymeric materials with enhanced thermal stability and properties optimized for PILF devices. This was achieved through a collaborative effort that resulted in high performance EO polyquinolines (introduced in Section 4) with high EO activity (> 29 pm/V at $1.3\text{ }\mu\text{m}$) and long-term thermal stability at $80\text{ }^{\circ}\text{C}$ for more than 1000 hours, as detailed in Section 5. In addition, we have pursued the structure/property relationships to fine-tune the wavelength of the absorption peak (λ_{max}) of NLO chromophores. This ability will ultimately allow us to take advantage of the significantly resonant-enhanced r_{33} values to reach the project goal ($r_{33} > 100$ pm/V at $1.3\text{ }\mu\text{m}$).

7.1 Motivation

It is well known that the linear EO effect in organic polymers is mainly electronic in origin even at low modulation frequencies (e.g. 1 kHz). This considerably facilitates the measurement of EO coefficients and the suitability to test new compounds for high speed modulation. The dispersion of electronic NLO susceptibilities are reasonably well described by the quantum mechanical two level model [16]. This is a function of intrinsic molecular properties, linear optical dispersion properties and the resonance frequency of the optical transition, ω_0 . The dispersion of the EO figure of merit n^3r is then, to first order, determined by a parameter proportional to the product of the dipole moment and the microscopic hyperpolarizability, $\mu\beta$.

In order to demonstrate the potential of organic materials, we present a comparison of a very well know and widely used NLO chromophore, DR1 (chromophore 1), with a recently developed chromophore for EO polymers (chromophore 2) [17]. Table 2 lists the relevant properties.

Table 2. Wavelength of maximum absorption and $\mu\beta$ for "standard" and "new generation" chromophores for EO polymers

| | Chromophore | λ_{\max} (nm) | $\mu\beta$ (10^{-48} esu) |
|---|-----------------------------------------------------------------------------------|--------------------------|---------------------------------|
| 1 |  | 455 | 580 |
| 2 |  | 744 | 15,000 |

As clearly seen in Table 2, microscopic properties are increased by more than an order of magnitude concomitant with an increase in λ_{\max} . Assuming similar number densities of chromophores, Figure 28 illustrates the dispersion behavior of the EO figure of merit for a typical DR1 side chain polymer and a similar polymer incorporating chromophore 2 from Table 2.

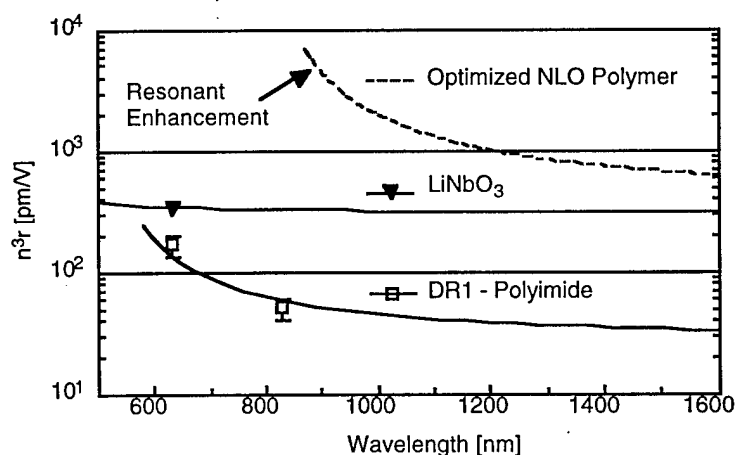


Figure 28. EO figures of merit for DR1 sidechain polyimide and an optimized polymer using chromophores of the new generation. A shift in absorption wavelength of 30 nm has been assumed when going from solution into bulk polymer phase. Extrapolations to wavelengths closer than 100 nm to λ_{\max} are not reliable since the two level model in this form is only valid outside of resonances. The dispersion for LiNbO₃ is given for comparison.

Figure 28 is a good illustration of the effects of resonant enhancement on EO figures of merit. The tremendous improvement in n^3r for the optimized EO polymer is due to not only the increased dispersion free properties, $\mu\beta$, of the new generation chromophores but also to the red shifted absorption bands toward the wavelength of interest (1.3 μm), which give rise to strong resonant enhancement. An r_{33} value of 55 pm/V at a wavelength of 1.3 μm has already been demonstrated using a polycarbonate composite with a chromophore very similar to chromophore 2 in Table 2 at about half the number density assumed in Figure 28 [17]. It is clear that resonantly enhanced EO polymers will have a tremendously beneficial impact on the development of PILF based devices.

As an example of the effect of resonant enhancement on the operation of a device, consider an amplitude modulator similar to that described in Section 6.3. If we calculate the modulation as a function of wavelength, we can simulate the effect of shifting the absorption peak to the operating wavelength. Using similar modeling techniques to those described earlier, we have estimated the improvement in modulation that can be realized. This estimation was done by altering the thickness of the EO polymer to provide a phase match at a particular wavelength (the applied modulating field remained constant) while taking into account the resonant enhancement of the EO coefficients. The results are shown in Figure 29.

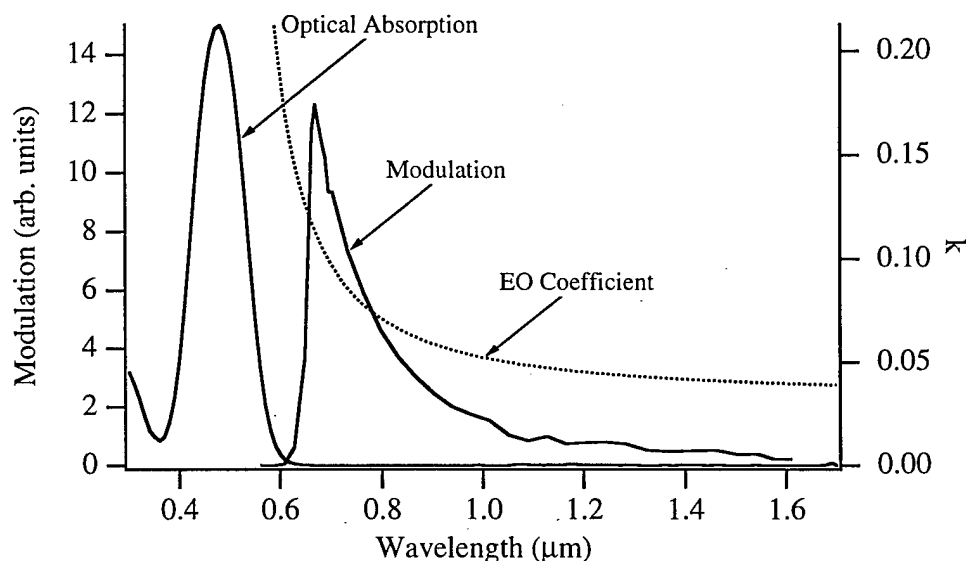


Figure 29. Estimate of the resonantly enhanced modulation in a PILF device operated close to an absorption peak.

In Figure 29 we see that the modulation can be greatly increased (by approximately an order of magnitude, compared to 1.3 μm) by operating close to the absorption peak. However, at a point approximately 200 nm away from λ_{max} , the loss increases rapidly and the modulation quickly drops off.

This figure indicates that potential to be realized in PILF devices utilizing highly active, resonantly enhanced EO polymers. However some caution should be exercised. Measurement of the loss away from absorption peaks is difficult and often unreliable. Techniques such as photothermal deflection spectroscopy must be employed for accurate measurements of this data.

7.2 Nonlinear Optical Chromophores

Several approaches can be followed to obtain NLO chromophores exhibiting larger $\mu\beta$ values (leading to polymers with large EO coefficients). These include introducing more effective electron withdrawing and donating groups and introducing longer π -conjugation. In both cases, the optical absorption at the operating wavelength is often a limiting factor. Indeed, for efficient operation of traditional EO devices, the optical absorption must be essentially zero. Therefore, development of new chromophores is often dictated by extremely stringent loss requirements and the use of chromophores with longer π -conjugation structures is limited due to the additional optical absorption associated with the shift in the absorption spectra.

Introducing a longer π -conjugation structure into a chromophore increases the molecular nonlinearity, β , by increasing the separation between the donor and acceptor in the NLO chromophore but with an associated increase of λ_{max} . The dispersion of the EO coefficient r_{33} can be approximated by a two level dispersion model [18].

$$r_{33} = \frac{4d_{33}}{n^4(\omega)} \frac{f_{\omega}^2 f_0}{f_{2\omega} f_{\omega'}} \frac{(3\omega_0^2 - \omega^2)(\omega_0^2 - \omega'^2)(\omega_0^2 - 4\omega'^2)}{3\omega_0^2(\omega_0^2 - \omega^2)^2}$$

Where ω is the frequency of the optical field used to measure r_{33} , d_{33} is the bulk second harmonic coefficient measured at fundamental frequency ω' , ω_0 is the frequency of the charge transfer band, and f are the local field factors of Onsager type. The singularity in the above equation as ω approaches ω_0 is the cause of the resonant enhancement of the EO coefficients. *Provided that the larger absorption loss can be tolerated*, a significant

enhancement of the EO coefficient, r_{33} , is possible by using an EO polymer containing NLO chromophores with λ_{\max} as close as possible to the use wavelength.

In order to realize highly efficient EO polymers that are capable of achieving the proposed project goal, we have selected several highly active heteroaromatic NLO chromophores for the incorporation into high temperature polyquinolines. Recently, Dr. Jen's group has demonstrated that very large nonlinearities can be achieved by employing heteroaromatic rings which have lower aromatic stabilization energy upon charge separation, or by using extended polyene π -bridge systems that have strong electron acceptors. Incorporation of these chromophores into polymer matrices in a guest/host configuration and their subsequent electric field poling has yielded materials with very large EO coefficients ($r_{33} = 45$ pm/V at a wavelength of 1.3 μm). These values are significantly larger than the value of 31 pm/V for commercially available LiNbO₃. However, the long-term alignment stability of these EO polymer systems was limited due to the low inherent thermal stability (< 175 °C) of these chromophores that prevents them from being processed and poled at higher temperatures. Dr. Jen's group has recently developed a facile approach to synthesize NLO chromophores with both enhanced nonlinearity and thermal stability. This synthetic method combines the advantages of using a thiophene ring and a triene as efficient conjugating moieties for easier charge separation, and a 2,2'-dimethyl-propyl group connected 6-membered ring system that provides a conformation-locked geometry of *trans*-triene to prevent the thermally induced *cis-trans* isomerization. This allows the synthesis of a series of NLO chromophores with broad variations of electron acceptors to fine tune linear absorption property (λ_{\max}) and the $\mu\beta$ product.

Chromophore (c) in Figure 30 with a conformation-locked *trans*-triene bridge possesses very good thermal stability at 225 °C. Furthermore, when this chromophore was doped (15 wt %) in a polyquinoline host and poled (210 °C with a poling field of 1.4 MV/cm), the resulting polymer had an electro-optic coefficient, r_{33} , of 27 pm/V measured at 1.3 μm which is consistent with the large molecular nonlinearity. The thermal stability of the poled polymer was demonstrated by heating the poled sample in a oven at 100 °C for over 1000 hours. The EO activity of the sample showed an initial drop to 75 % of its original value within 80 hours then remained unchanged for the duration of the test.

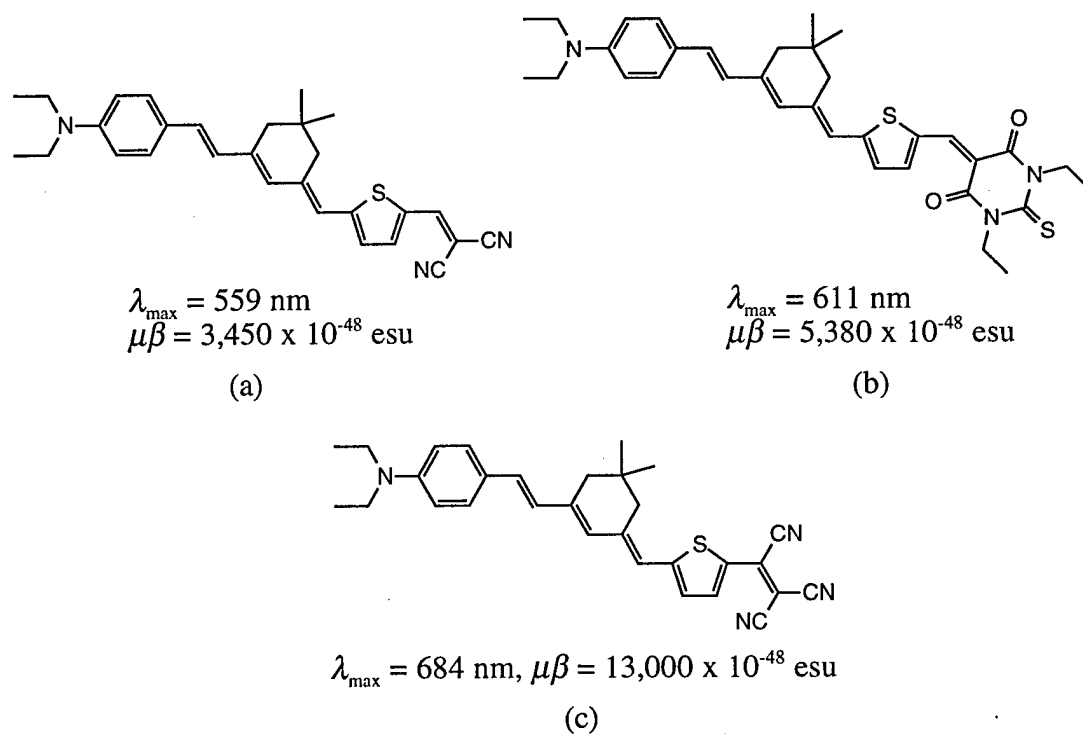


Figure 30. Variations of conformation-locked chromophores with enhanced nonlinearity and thermal stability.

Using the conformation-locked bridge approach described above, Dr. Jen's group has developed a series of donor-acceptor substituted chromophores (Figure 31) with completely ring-locked polyene bridges. By quenching the lithiated product of 4-bromo-N,N-diethylamino aniline with 3-ethoxy-2-cyclohexenone and 7-methoxy-3,4,4a,5,6-pentahydronaphthalen-2-one, then condensation with malononitrile and 3-phenyl-5-isoxazolone gave compounds (a) through (c) of Figure 31, respectively. These chromophores possess high nonlinearity, good thermal, chemical, and photochemical stability. These chromophores will be further optimized by extending their conjugation lengths through the construction of thiophene linkages and be appropriately functionalized for attachment onto high temperature polyquinolines for the evaluation of their EO properties.

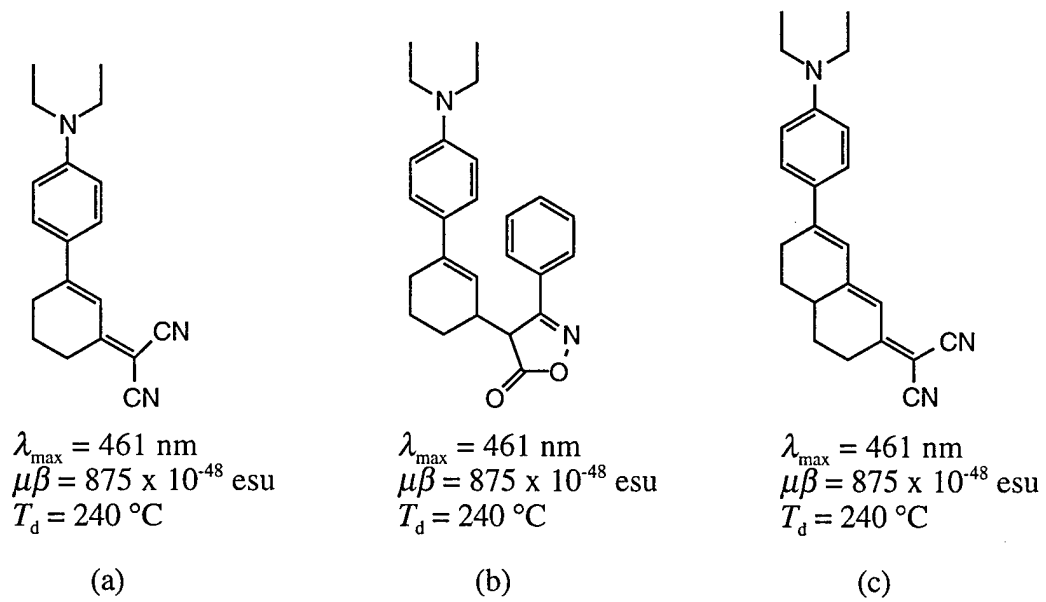


Figure 31. Chromophores with ring-locked polyene bridges.

8. Future Work

During future work, under a Phase II effort or otherwise, we intend to continue the development of EO polyquinolines, including the development of sidechain materials and materials incorporating more highly active chromophores. More specifically, we will concentrate on the following issues:

- Further development of highly active chromophores with large $\mu\beta$ products.
- Development of sidechain EO polyquinolines materials with more pronounced resonant enhancement of the optical nonlinearities at near IR wavelengths.
- Optimization of the thermal stability and the mechanical properties of the material
- Investigation and improvement of the compatibility of the chromophores and polymer.
- Detailed characterization of all newly developed materials, including complete characterization of both the linear and nonlinear optical properties.
- Large scale synthesis of promising EO polymer materials for incorporation into device structures.
- Use of PILF structures for long term analysis of the thermal and photochemical stability of these materials.
- Further development of a modulators suitable for Air Force use incorporating these new materials.

These issues are discussed further in the following sections.

8.1 Development of Highly Active EO Polymers

During future efforts we will further develop the materials we have identified during this Phase I effort and continue to pursue additional materials exhibiting even larger $\mu\beta$ values. Several promising chromophores have already been developed and incorporated into guest-host polyquinolines, these have been thoroughly described in the previous sections. In addition, other materials have been developed but not yet fully characterized. We will concentrate on these new materials and their incorporation into sidechain polyquinolines.

Figure 32 and Figure 33 illustrate two proposed synthesis schemes for the realization of sidechain polyquinoline materials. These two schemes differ in the attachment of the chromophore. The scheme shown in Figure 32, prefunctionalization, involves the incorporation of the chromophore prior to the completion of the polymerization while the scheme shown in Figure 33, postfunctionalization, involves the incorporation of the chromophore following the completing of all other synthesis steps. This second scheme

has the obvious advantage of isolating the chromophores from a number of potential threatening chemical procedures involved in the synthesis of the polyquinoline backbone. Therefore, this scheme may allow the incorporation of a number of chromophores that would otherwise not be able to be incorporated into sidechain polyquinolines.

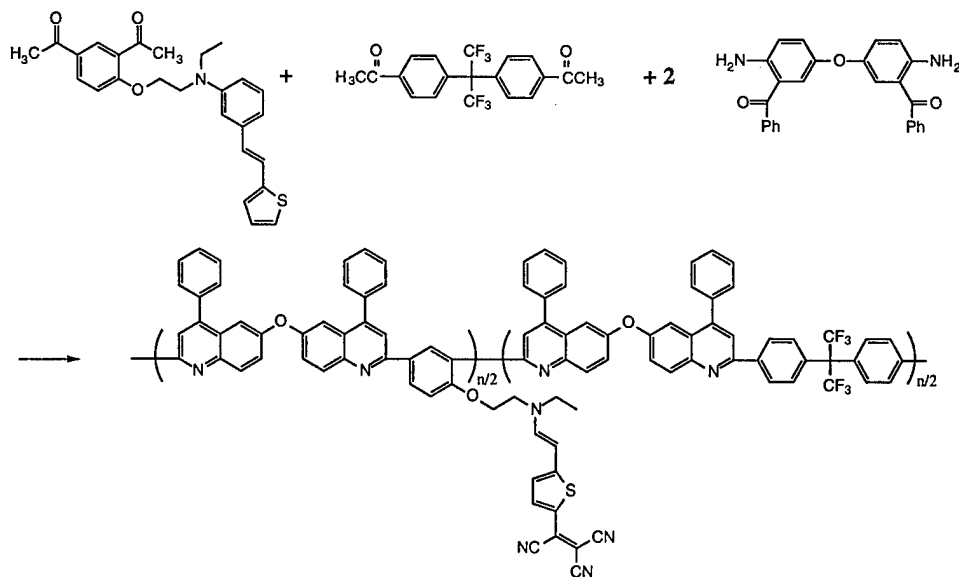


Figure 32. Post-functionalized polyquinoline.

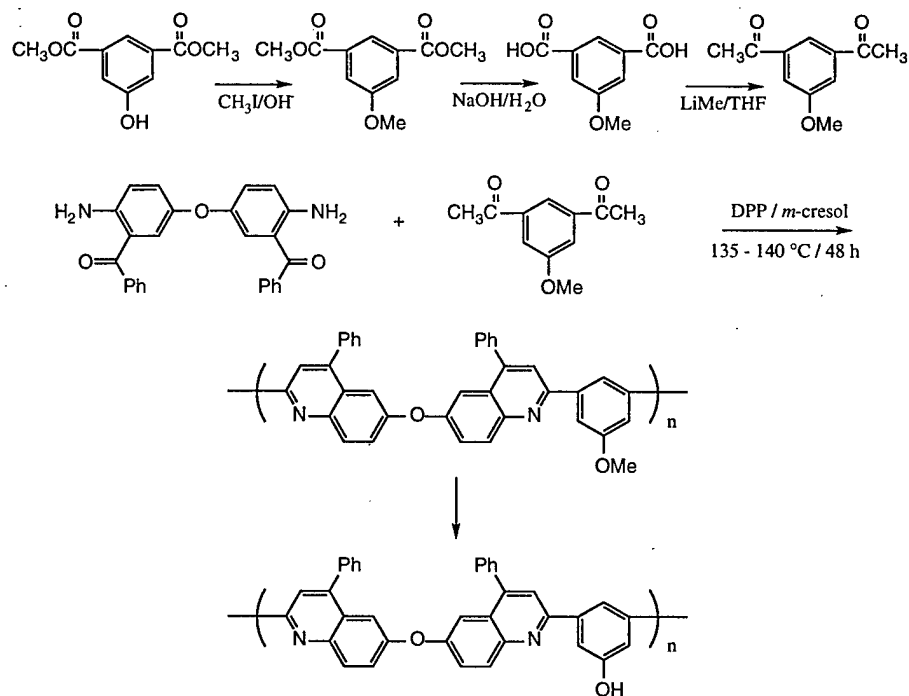


Figure 33. Pre-functionalized polyquinoline.

Additionally, we plan to investigate techniques to optimize the thermal stability and the mechanical properties of these materials. The thermal stability will be greatly enhanced by the development of sidechain materials, as opposed to guest-host mixtures. In addition, the development of chromophores with better thermal stability and polymer systems with higher glass transition temperatures will yield more stable materials. Of course, there is often a relationship between chromophore concentration and glass transition temperature. We will investigate this relationship and attempt to optimize the materials. It may be necessary to make tradeoffs between T_g and EO coefficients based on particular applications. Our analysis of the relationship between these properties will allow these tradeoffs to be made for these individual applications. The mechanical properties are of interest for use in deposition procedures such as the liftoff method discussed earlier. For this technique, the polymer must be very robust. The guest-host mixtures developed for the Phase I effort were compatible with this technique but did present a few difficulties, primarily with curling and wrinkling during the deposition onto the final substrate. During future work, we will more fully investigate these issues and attempt to solve them.

There are a number of issues involving the incorporation of high $\mu\beta$ product chromophores into polymers. Often, saturation effects are observed and the resulting EO coefficients are far lower than expected based on calculations. This has been attributed to chromophore-chromophore interactions and some techniques to yield higher EO coefficients have recently been proposed [19]. The majority of the work related to this issues has been focused on guest-host systems, the reasoning being that the effects would be more pronounced in these cases. However, similar issues exist with sidechain materials. We intend to investigate these relationships and determine the optimum chromophore concentrations for our particular material system. This will result in an optimized EO polyquinoline with the largest possible nonlinearity.

Following identification of an appropriate material which exhibits high thermal stability and EO activity; an effort to perform large scale production will be made. While well suited for development work, university-based research labs are not particularly appropriate for scale-up and production. For this reason, we intend to pursue outside firms to assist with large scale production. Organizations such as the IBM Almaden Research Center or small companies such as Chromophore Inc. and Adtech will be contacted to assist in this area. Close contact will be maintained between the university development team and the scale-up team to ensure efficient transfer of the synthesis techniques.

8.2 Material Characterization

8.2.1 Linear and Nonlinear Optical Properties

During future efforts we will pursue the characterization of new generations of EO polymers using several different methods to quantify both linear and nonlinear properties.

Critical for the development and use of resonantly enhanced materials is the precise measurement of the optical absorption outside of the actual absorption band. Measurement of this absorption is typically below the noise level of traditional spectrophotometers and therefore difficult to determine without complex waveguiding experiments. The UC Davis group has recently implemented a photothermal deflection spectrometer and is in the process of optimizing it for these measurements. This device is ideal for measurement of optical absorption at these long wavelengths and will give us valuable insight in residual absorption at the critical wavelengths. We intend to utilize this equipment to investigate a number of materials and precisely determine the optical loss at the operating wavelength. These results will provide valuable insight which will allow a more thorough understanding of the tradeoffs associated with working at wavelengths close to the absorption band.

In addition, we will continue to utilize and develop the more traditional measurement techniques for the determination of the optical properties. These include spectroscopic ellipsometry, spectrophotometry, and the Fabry-Perot reflection technique for determination of the electro-optic coefficients. Finally, the PILF structure itself will be used for the evaluation and determination of the optical properties in an actual device configuration.

8.2.2 Long Term Stability

In addition to the characterization of the linear and nonlinear optical properties, we will employ the PILF structure to further quantify the long term thermal and photochemical stability of the newly developed EO polymers.

A great deal of effort has been put into research relating to the relaxation of poling induced molecular orientation in EO polymers. These efforts have led to the development of high T_g polymers and chromophores and more stable polymer environments which have largely eliminated the early concerns about thermal stability. However, another potential problem is the photochemical stability of the EO polymers, that is, their ability to resist chemical

degradation or breakdown in the presence of light. Although this effect is most often noted with high incident optical power densities, damage has also been observed at lower powers over long periods [20]. The causes of this decay are still largely unknown and are therefore of concern to all EO polymer based devices.

The PILF structure is ideally suited to study both the thermal stability and photochemical stability of EO polymers. The self-aligned design of the PILF structure makes it an ideal tool for the long term analysis of properties such as these. For these long term tests, the PILF structure has many of the benefits of a standard polymer waveguide structure, without the added complexity of buffer layers. It is the addition of these buffer layers that makes the fabrication and poling of three layer polymer waveguides so complicated and their use as a characterization tool difficult.

During future efforts we will continue to use the PILF structure to perform long term analysis of EO polymers. The location of the transmission dip will be monitored as a probe of any changes in the poling induced birefringence and the amplitude of the modulation will be monitored as a probe of the EO coefficients. In addition optical loss through the device will be monitored. By recording these parameters as a function of incident power, we will be able to determine if any observed changes are due simply to slight poling relaxations or other effects, such as photochemical degradation.

8.3 PILF Device Development

One of the limitations we have come up against is the limited interaction length of the available half-couplers. Commercially available half-couplers have an interaction length of approximately 1 mm which is sufficient for material characterization and proof-of-concept devices but not for practical devices. For low voltage modulators, half-couplers with interaction lengths on the order of 1 cm will be required.

We have recently begun a development effort to realize these longer interaction lengths. This effort involves the use of silicon v-groove technology to precisely define a fiber groove in a silicon substrate. The ability to accurately define this groove allows the fabrication of half-couplers with much longer interaction regions than is possible with glass block half-couplers. A schematic of a silicon v-groove based PILF structure is shown in Figure 34.

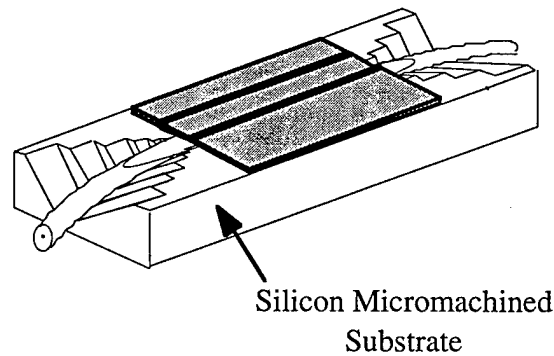


Figure 34. PILF device fabricated on a silicon micromachined half-coupler.

The development of these improved half-couplers will allow the development of PILF structures and devices with much narrower transmission dips. In addition to lowering the drive voltage of PILF modulators, these narrow dips will allow the realization of filters and other devices suited for the narrow bandwidth requirements of today's WDM systems.

8.4 Commercialization Plan

On October 20, 1997, a new company, Optical Networks, Incorporated (ONI), was formed to develop commercial markets for Optivision's expertise in photonics. ONI's primary objective is to focus Optivision's research, development and systems expertise in photonics on commercial optical network products for the emerging optical telecommunications and data communications markets.

Effective October 29, 1997, ONI and Optivision entered into a license agreement that provides ONI with exclusive access to Optivision's photonics technology. On January 13, 1998, two leading first tier venture capital firms, Kleiner Perkins Caulfield & Byers (KPCB), and Mohr, Davidow (MD), made substantial investments in ONI. Coincident with this investment, Hugh Martin, former COO of 3DO, Inc., and former senior executive at Apple Computer, Inc., became ONI's Chief Executive Officer.

All key Optivision photonics employees became ONI employees at the end of February, 1998. ONI currently has approximately 25 employees, with plans for substantial rapid growth in the product development area. Initial product development focus will be on restoration switching systems for WDM networks, however development of next generation photonics products resulting from the technologies developed under research efforts such as this one is also anticipated.

The Optivision photonics employees who have joined ONI include outstanding scientists and engineers with many years of technical experience in photonics, optical networking, and related fields. This technical expertise, coupled with the substantial venture capital investment, and a new senior management team that has a proven track record in commercialization of high technology products, will enable ONI to fully exploit newly developed photonics technology.

An additional resource for commercialization is the KPCB "Keiretsu" network of shared information and knowledge. As a new member of the KPCB Keiretsu, ONI will be able to share experiences, insights, knowledge, and information with a network of more than 175 companies and thousands of executives. The KPCB Keiretsu includes leading high technology companies such as Ascend Communications, Compaq Computers, Intuit, and Sun Microsystems.

The PILF structure presents the opportunity to develop a variety of devices, including amplitude modulators, phase modulators, and wavelength filters, with truly significant advantages over competing technologies. These advantages include a rugged design and a low cost package that eliminates the need for costly, time consuming pigtailed procedures. The continued development of appropriate EO polymers during future efforts will enable practical PILF devices to be realized.

Optivision had an ongoing effort in the area of RF photonics, including the development of optical amplifiers, RF optical modulators, and low cost LiNbO_3 packaged devices. This effort has now been fully transferred to ONI. The development of PILF devices in general meshes perfectly with the overall development path for ONI's RF photonic products.

During future efforts, ONI will pursue a variety of options for manufacturing and distribution of these devices. These options include collaborations with organizations capable of large scale EO polymer synthesis and further development of in-house manufacturing capabilities. As an example of the latter, we are currently pursuing the fabrication of the silicon half-couplers previously discussed in order to obtain more precise control over the fabrication parameters. This development will be directly applicable to the commercialization of the PILF devices described here.

8.5 Conclusions

We have successfully completed all tasks in the Phase I effort. The objective of the effort was to develop highly active EO polymers for in-line fiber photonic devices. The major accomplishments of the Phase I effort were:

- Procurement of a significant quantity of a guest-host polyquinoline mixture for development of processing, characterization, and fabrication techniques suitable for future polyquinolines. This material had an r_{33} of 29 pm/V at 1.3 μm and was stable at 80 °C for more than 1000 hours.
- Development of processing, characterization and fabrication techniques compatible with polyquinoline materials. These techniques will be compatible with future polyquinolines and will allow the rapid characterization and device level testing of those materials.
- Successful fabrication of PILF structures incorporating the guest-host polyquinoline. Device operation of an amplitude modulator at 10 MHz with a signal to noise ratio > 70 dB was demonstrated.
- Successful synthesis of highly active NLO chromophores suitable for incorporation into sidechain polyquinolines.
- Demonstration of the dynamic range capabilities of PILF modulators. The spurious free dynamic range of a device was fully evaluated and the potential to exceed that of Mach-Zehnder devices was shown.

This Phase I effort resulted in the incorporation of some very exciting materials into the PILF structure and demonstrated the potential for future polyquinolines which will incorporate more highly active chromophores in a sidechain configuration. In future work, whether funded under a Phase II effort or some other source, we will continue the development of these materials with the ultimate goal being the development of practical PILF-based EO devices.

9. References

1. D. Yu, A. Gharavi, and L. Yu, "A Generic Approach to Functionalizing Aromatic Polyimides for Second-Order Nonlinear Optics," *Macromolecules*, vol. 28, p. 784 (1995).
2. S. Ermer, J. F. Valley, R. Lytel, G. F. Lipscomb, T. E. Van Eck, D. G. Girton, D. S. Leung, and S. M. Lovejoy, in Organic and Biological Optoelectronics, P. M. Rentzepis, ed., *Proc. SPIE*, vol. 1853, p. 183 (1993).
3. A. K-Y. Jen, V. P. Rao, T. Chen, Y. Cai, K. J. Drost, Y.-J. Liu, J. T. Kenney, R. M. Mininni, P. V. Bedworth, S. R. Marder, and L. Dalton, "High Performance Chromophores and Polymers for E-O Applications," in *Organic Thin Films for Photonics Applications*, vol. 21, 1995 OSA Technical Digest Series (Optical Society of America, Washington DC, 1995), p.251.
4. G. Lindsay, J. Stenger-Smith, A. Chafin, R. Hollins, L. Merwin, R. Yee, R. Nissan, M. Nadler, R. Henry, K. Wynne, P. Ashley, L. Hayden, and W. Herman, "New Polymers for Second-Order Nonlinear Optics," in *Organic Thin Films for Photonics Applications*, vol. 21, 1995 OSA Technical Digest Series (Optical Society of America, Washington DC, 1995), p.247.
5. T. Verbiest, D. M. Burland, M. C. Jurich, V. Y. Lee, R. D. Miller, and W. Volksen, *Science*, vol. 268, p. 1604 (1995).
6. K. D. Singer, M. G. Kuzyk and J. E. Sohn, "Second-order nonlinear-optical processes in orientationally ordered materials: relationship between molecular and macroscopic properties," *J. Opt. Soc. Am. B*, vol. 4, pp. 968-976 (1987).
7. C. C. Teng and H. T. Man, "Simple reflection technique for measuring the electro-optic coefficient of poled polymers," *Appl. Phys. Lett.*, vol. 56, no. 18, pp. 1734-1736 (1990).
8. D. R. Yankelevich, R. A. Hill, A. Knoesen, M. A. Mortazavi, H. N. Yoon, and S. T. Kowel, "Polymeric modulator for high frequency optical interconnects," *IEEE Photon. Technol. Lett.*, vol. 6, no. 3, pp. 386-389 (1994).
9. R. M. A. Azzam and N. M. Bashara, *Ellipsometry and Polarized Light*, (North-Holland, Amsterdam, 1977), pp. 282-340.
10. A. Knoesen, "Simple approach to reflectance analysis of birefringent stratified films," *Appl. Opt.*, vol. 30, no. 28, pp. 4017-4018 (1991).
11. MATLAB 4.0, Copyright 1994, The Math Works Inc., Natick, MA 01760.
12. D. Morichère, P. A. Chollet, W. Fleming, M. Jurich, B. A. Smith, and J. D. Swalen, "Electro-optic effects in two tolane side-chain nonlinear-optical polymers:

comparison between measured coefficients and second-harmonic generation," *J. Opt. Soc. Am. B*, vol. 10, no. 10, pp. 1894-1900 (1993).

13. J. I. Thackara, G. C. Bjorklund, W. Fleming, M. Jurich, B. A. Smith, and J. D. Swalen, "A polymeric electro-optic phase modulator for broadband data communication," *Proc. SPIE, Nonlinear Optical Properties of Organic Materials VI*, vol. 2025, pp. 564-573 (1993).
14. R. A. Hill, G. C. Bjorklund, S. A. Hamilton, D. R. Yankelevich, and A. Knoesen, "Polymeric in-line fiber modulator using novel processing techniques," *Optical Fiber Communication '96 Technical Digest*, pp. 166-167 (1996).
15. Ph. Prêtre, L.-M. Wu, R. A. Hill, and A. Knoesen, "Characterization of electro-optic polymer films by use of decal-deposited reflection Fabry-Perot microcavities," *J. Opt. Soc. Amer. B*, vol. 15, no. 1, pp. 379-392 (1998).
16. J. L. Oudar and D. S. Chemla, "Hyperpolarizabilities of the nitroanilines and their relations to the excited state dipole moment," *J. Chem. Phys.*, vol. 66, pp. 2664-2668 (1977).
17. M. Ahlheim, M. Barzoukas, P. V. Bedworth, M. Blancharddesce, A. Fort, Z. Y. Hu, S. R. Marder, J. W. Perry, C. Runser, M. Staehelin, and B. Zysset, "Chromophores with strong heterocyclic acceptors - a poled polymer with a large electro-optic coefficient," *Science*, vol. 271, pp. 335 (1996).
18. K. D. Singer, S. L. Lalama, J. E. Sohn, and R. D. Small, in *Nonlinear Optical Properties of Organic Molecules and Crystals*, D. S. Chemla, and J. Zyss, eds., (Academic Press, Orlando, 1987), pp. 437-468.
19. A. W. Harper, S. Sun, L. R. Dalton, S. M. Garner, A. Chen, S. Kalluri, W. H. Steier, and B. H. Robinson, "Translating microscopic optical nonlinearity into macroscopic optical nonlinearity: the role of chromophore-chromophore electrostatic interactions," *J. Opt. Soc. Am. B*, vol. 15, no. 1, pp. 329-337 (1998).
20. M. A. Mortazavi, H. N. Yoon, and C. C. Teng, "Optical Power Handling Properties of Polymeric Nonlinear Optical Waveguides," *J. Appl. Phys.*, vol. 74, no. 8, pp. 4871-4876 (1993).